Summer compound heatwaves over China: projected changes at different global warming levels and related physical processes

Climate Dynamics
https://doi.org/10.1007/s00382-023-07001-4

ORIGINAL ARTICLE

Summer compound heatwaves over China: projected changes at different global warming levels and related physical processes

Mingming Zhang[1] · Buwen Dong[2] · Reinhard Schiemann[2] · Jon Robson[2]

Received: 12 May 2023 / Accepted: 13 October 2023

Abstract

Based on the multi-model ensemble mean of CMIP6 simulations, the future changes in frequency, intensity and duration of Compound (both daytime and nighttime) heatwaves (HWs) in summer over China at various global warming levels (GWLs) under the SSP3-7.0 and SSP5-8.5 are assessed. HWs over China become more frequent and hotter, and the duration of HWs becomes longer compared to those in the recent climate. The magnitudes of these changes are primarily dependent on GWLs, but they are not very sensitive to the scenarios. At 4 ℃ GWL, the frequency of HWs increases by more than fivefold under both scenarios, and the intensity (duration) of HWs averaged under the two scenarios is 2.28 ℃ hotter (3.59 days longer) than the one in the recent climate over the entire China. Meanwhile, the maximum duration of HW events can reach more than 25 days in summer in comparison with 8 days in the recent climate. The changes in HW properties are regionally dependent at the four GWLs. For example, the largest increase in HW frequency is over the Northwest China, the largest increase in intensity in HWs is seen over the Northeast and Northwest, and the largest increase in HW duration is over the Southwest China. The extreme rare events (50-year and 100-year events) in the recent climate would become the norm over China and four sub-regions at 4 ℃ GWL. Overall, seasonal mean warming dominates the changes in HW properties over China at the different GWLs. The seasonal mean warming in summer across China is related to the increases of longwave radiation, partly due to increase in greenhouse gas forcing and partly resulted from increased water vapor and the increase of shortwave radiation (under the SSP5-8.5) over eastern China related to decreases in aerosols and total cloud cover. Furthermore, the regional variations in the water vapor over China are consistent with atmospheric circulation changes. The seasonal mean surface warming results in enhanced upward sensible and latent heat fluxes, leading to increased summer mean daily maximum and minimum of near-surface air temperature and the enhancement of HWs properties over the entire China. Changes of shortwave radiation tend to play a weaker role for surface warming under the SSP3-7.0 than those under the SSP5-8.5, which is related to increased aerosol changes under the SSP3-7.0.

Keywords Summer compound heatwaves · Future projections · Global warming levels · China

1 Introduction

Heatwaves (HWs) are weather events characterized by extreme hot surface air temperature anomalies that persist for several days (Coumou and Rahmstorf 2012; Seneviratne et al. 2014; Sun et al. 2014; Perkins 2015), and thus leading to devastating impacts on human health, agriculture, economy, and natural ecosystems. (e.g., Robine et al. 2008; Coumou and Rahmstorf 2012; Seneviratne et al. 2014; Hatfield and Prueger 2015; Lesk et al. 2016, Kornhuber et al. 2020; Bras et al. 2021; Alizadeh et al. 2022). For instance, a record-breaking HW hit central Europe in the summer of 2003 with a reduction of cereal production over 23 million tonnes compared to 2002. It caused a destruction of large areas of forests and the economic losses were estimated to exceed 13 billion euros (De Bono et al. 2004). According to the World Meteorological Organization, the number of deaths related to HWs during 2001–2010 increased by 2300% compared with the number during 1991–2000 (WMO 2013). Hence, these adverse

✉ Mingming Zhang
mingming.zhang@pgr.reading.ac.uk

[1] Department of Meteorology, University of Reading, Reading, UK

[2] National Centre for Atmospheric Science, Department of Meteorology, University of Reading, Reading, UK

Published online: 07 November 2023

impacts of HWs highlight the importance of studying how HWs will change in response to global warming.

In recent decades, the occurrence of heatwaves (HWs) has been more frequent across the world (Donat et al. 2013; Su and Dong 2019a; Liao et al. 2021; Perkins-Kirkpatrick and Lewis 2020; Singh et al. 2021). Regionally, HWs are also becoming more frequent and severe over China (Piao et al. 2010; Ye et al. 2014; Sun et al. 2014; Wang et al. 2017; Zhao 2020; Wang and Yan 2021). Since the late 1990s, the frequency of the extreme HWs has increased most significantly over North China and central northern China, while the occurrence of mild HWs has increased most significantly over Jianghuai and South China (Xie et al. 2020). The hottest summer during period 1955–2013 over Eastern China took place in 2013 and the average number of heatwave days was 31 days, which was over twice as many as the climatological average of 1955–1984 (Sun et al. 2014). Li et al. (2021) showed that the occurrence of HWs with both intensity and duration exceeding the 100-year return level increased by 16% in China during 1998–2017 compared with the period 1961–1997. According to the occurrence time and different impacts, HWs can be divided into Compound HWs (hot in both day and night), Daytime HWs and Nighttime HWs (Gershunov et al. 2009; Luo et al. 2022). Chen and Li (2017) found that Compound HWs and Nighttime HWs increased significantly in frequency, duration, intensity and areal extent during 1961–2010. Some recent studies have shown that anthropogenic forcing plays the dominant role for the decadal changes of HWs over China (Freychet et al. 2018; Chen et al. 2019; Su and Dong 2019a) in which the greenhouse gas changes influence all three types of HWs and the anthropogenic aerosol has significant impacts on Daytime HWs (Su and Dong 2019a).

As the global mean surface temperature (GMST) increases under different future forcing scenarios, it is expected that there will be an increase of warm extremes over China (Zhou et al. 2014; Hu and Sun 2020; Chen and Dong 2021). Previous studies mainly focused on the future changes of HWs, defined by daytime maximum temperature (Guo et al. 2017; Kong et al. 2020; Zhang et al. 2020). For example, by applying the dynamical downscaling simulations of RegCM4, the ensemble results showed that the increasing rates of HWs are 0.33 per decade for frequency and 0.38 ℃ per decade for magnitude under RCP4.5 scenario over China towards the end of twenty-first century (Xie et al. 2021). Wang et al. (2019) also used the Weather Research Forecasting (WRF) model simulations with initial and boundary conditions from four CMIP5 GCMs to investigate future changes of HWs over China. They found that HWs will intensify more rapidly than the present period and the strong HWs with prolonged durations and more severe magnitudes will occur more frequently in the future. The frequency of extreme HWs will also increase rapidly with global warming (Sun et al. 2018).

In contrast to the influence of HWs, which occur on daytime or nighttime, Compound HWs combine both Daytime HWs and Nighttime HWs and can have severe impacts on society (Chen and Zhai 2017; An and Zuo 2021). Wang et al. (2020) suggested that the compound HWs will be the most frequent type that populations are exposed to after 2030 in the Northern Hemisphere. Hence, it is also worthwhile to focus on the future changes of Compound HWs over China. However, a very limited number of studies have discussed it. Su and Dong (2019b) investigated the future changes between the mid-twenty-first century (2045–2055) and present day (1994–2011) by using an atmospheric general circulation model coupled to an ocean mixed layer model under the RCP4.5. The frequency of Compound HWs in the future is projected to be 4–5 times as many as that in the present day. The intensity and duration are projected to be double relative to the present day. The frequency of Compound HWs at the end of the twenty-first century (e.g., 2081–2100) relative to the present day (e.g., 1995–2014) is projected to increase across the whole of China, but the greatest changes occur over Northwest China and southern China (Xie et al. 2022). However, these previous studies mainly focused on a fixed time period in future projections.

In December 2015, the parties of the United Nations Framework Convention on Climate Change (UNFCCC 2015) signed the Paris Agreement and proposed a goal as 'holding the increase in the global average temperature to well below 2.0 ℃ above pre-industrial levels and pursuing efforts to limit the temperature increase to 1.5 ℃ above pre-industrial levels.'. Accordingly, the evaluation of future projections based on target global warming levels (GWLs), instead of a fixed time period, has become increasingly important. However, based on projections of future emissions, it is thought that there is only a 5% chance to limit GMST warming to below 2 ℃ (Raftery et al. 2017). In particular, Raftery et al. (2017) projected that the likely range of GMST increase is 2.0–4.9 ℃ with a median of 3.2 ℃ by

Table 1 The list of models used in this study

	Model	Resolution (lon × lat)	Members
1	BCC-CSM2-MR	320 × 160	1
2	FGOALS-g3	180 × 80	1
3	CNRM-CM6-1	256 × 128	1
4	ACCESS-ESM1-5	192 × 144	3
5	ACCESS-CM2	192 × 144	3
6	MIROC6	256 × 128	3
7	IPSL-CM6A-LR	144 × 143	1
8	MRI-ESM2-0	320 × 160	5
9	NorESM2-LM	144 × 96	1

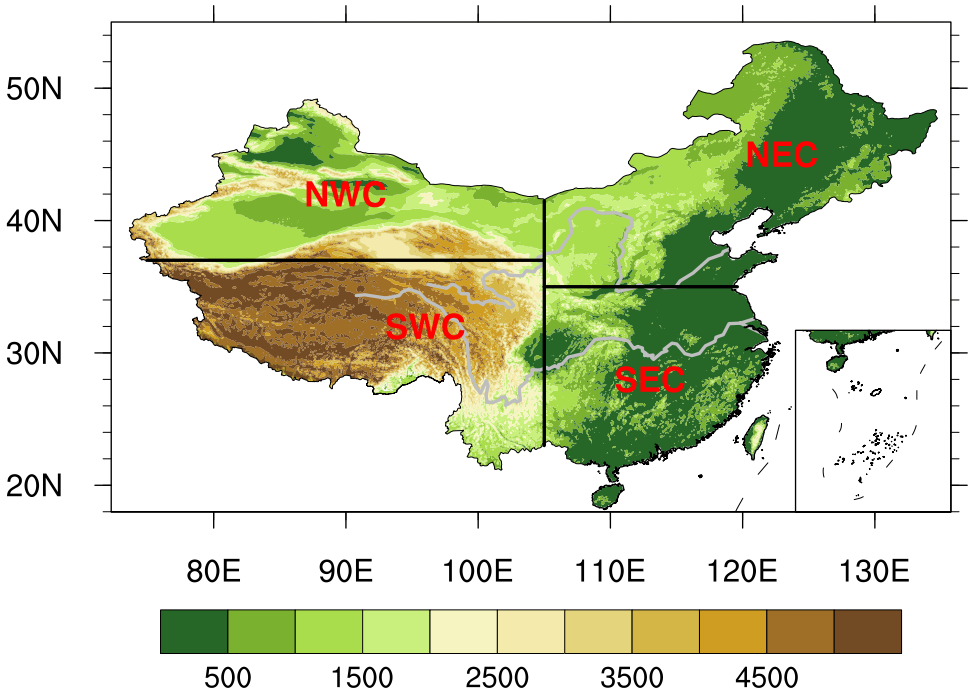

Fig. 1 The topography (units: m) over the study regions. The subregions analyzed in the study are distinguished by black lines and they are Southeast China (SEC), Northeast and North China (NEC), Northwest China (NWC) and Southwest China (SWC)

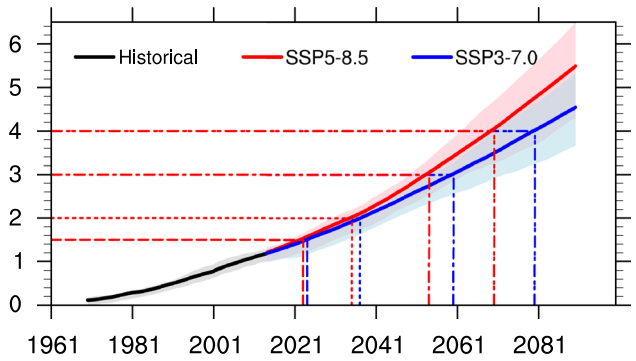

Fig. 2 Time series of 20-year moving global mean surface temperature anomalies (relative to 1850–1900 pre-industrial period) from CMIP6 models. Black line is historical simulations and blue (red) line represent SSP3-7.0 (SSP5-8.5) scenario. Solid lines indicate the multi-model ensemble mean, and shading the interquartile ranges. Vertical dashed lines indicate the calendar year for the ensemble mean to reach 1.5 ℃, 2 ℃, 3 ℃ and 4 ℃ GWLs

the end of the twenty-first century. Furthermore, only 14% of the temperature related discussions in the IPCC AR6 report are about GWLs exceeding 2 ℃ (Jehn et al. 2022), and the impacts of higher end warming scenarios of 3 ℃ and above are less emphasized (Jehn et al. 2021). Hence, it is necessary to focus on the future changes at the target GWLs at 1.5 ℃, 2 ℃, 3 ℃ and 4 ℃ to assist the government in making policy decisions and mitigating the risks associated with these hot extremes.

The Coupled Model Intercomparison Project Phase 6 (CMIP6) models provide the most up-to-date simulations of future climate and show a general improvement in simulating extreme climate in China compared with previous phases (Chen et al. 2020). Therefore, to better understand the future changes in Compound HWs over China under different GWLs, this study aims to quantify the magnitude of changes in Compound HWs and identify the related physical processes based on CMIP6 multi-model ensembles. The paper is organized as follows: Sect. 2 describes the data and methods used in this study. Sect. 3 shows the changes of Compound HWs at the 1.5 ℃, 2 ℃, 3 ℃ and 4 ℃ GWLs. The physical processes related to the changes of HW properties are elucidated in Sect. 4. The conclusions and discussions are summarized in Sect. 5.

2 Data and methods

2.1 Data

This study uses the historical simulations and future projections from CMIP6 (Eyring et al. 2016). The historical simulations cover the past period 1850–2014. The future projections cover the period 2015–2100 with different scenarios of external forcings. Here, we use two scenarios. The first is the SSP3-7.0, which has a medium to high radiative forcing of 7.0 W m^{-2} by 2100. The SSP3-7.0 has a particularly high aerosol emissions and it fills a gap between the RCP6.0 and RCP8.5 in CMIP5 forcing pathways (IPCC 2022). The second scenario used is the SSP5-8.5 which represents the highest forcing pathway with a radiative forcing

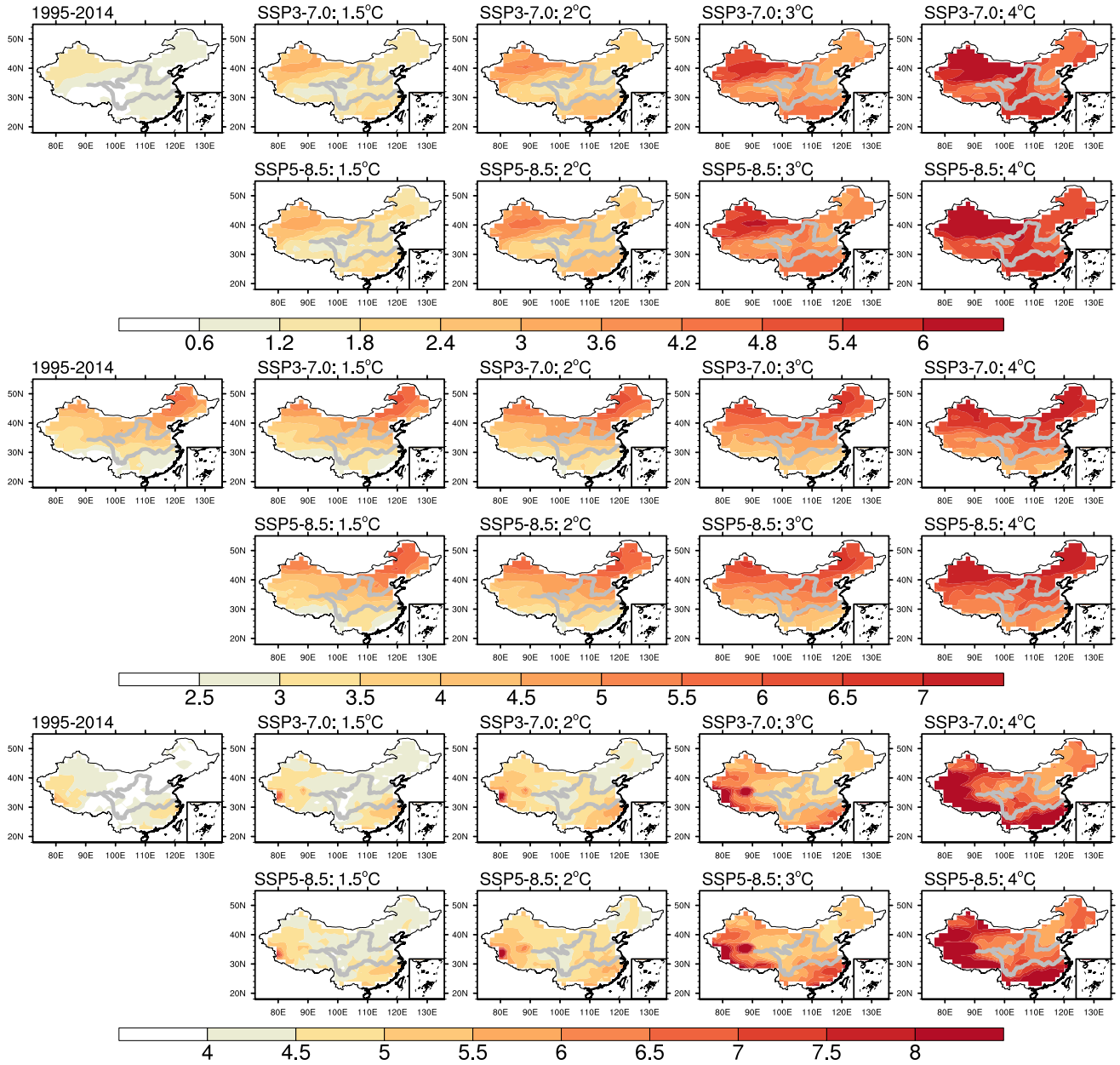

Fig. 3 The simulated spatial patterns of the frequency (top two rows, units: events a^{-1}), intensity (middle two rows, units: °C) and duration (bottom two rows, units: days) of Compound HWs in the recent climate (1995–2014), and at the 1.5 ℃, 2 ℃, 3 ℃ and 4 ℃ GWLs under the SSP3-7.0 and SSP5-8.5

of 8.5 W m^{-2} in 2100 (O'Neill et al. 2016). The models and ensemble numbers used are listed in Table 1. These models can well represent the historical temperature distributions over China (Yang et al. 2021; You et al. 2021).

The model outputs of daily minimum temperature (Tmin), maximum temperature (Tmax), daily mean temperature, as well as monthly radiation and atmospheric circulation variables are analyzed in the following sections. In order to calculate the multi-model ensemble mean, the bilinear interpolation method is used to regrid the model outputs to a common 1.5° × 1.5° grid to facilitate the intercomparison. The ensemble members of historical simulations and future projections in each model are the same. The HWs properties of each ensemble member are calculated individually. To treat each model equally, the multi-member mean is calculated in each model first and then the multi-model ensemble mean is derived by all models.

Based on the topography and regional climate over China (Song et al. 2011), we focus on the changes over the entire China and its four subregions (Fig. 1), which are Northeast

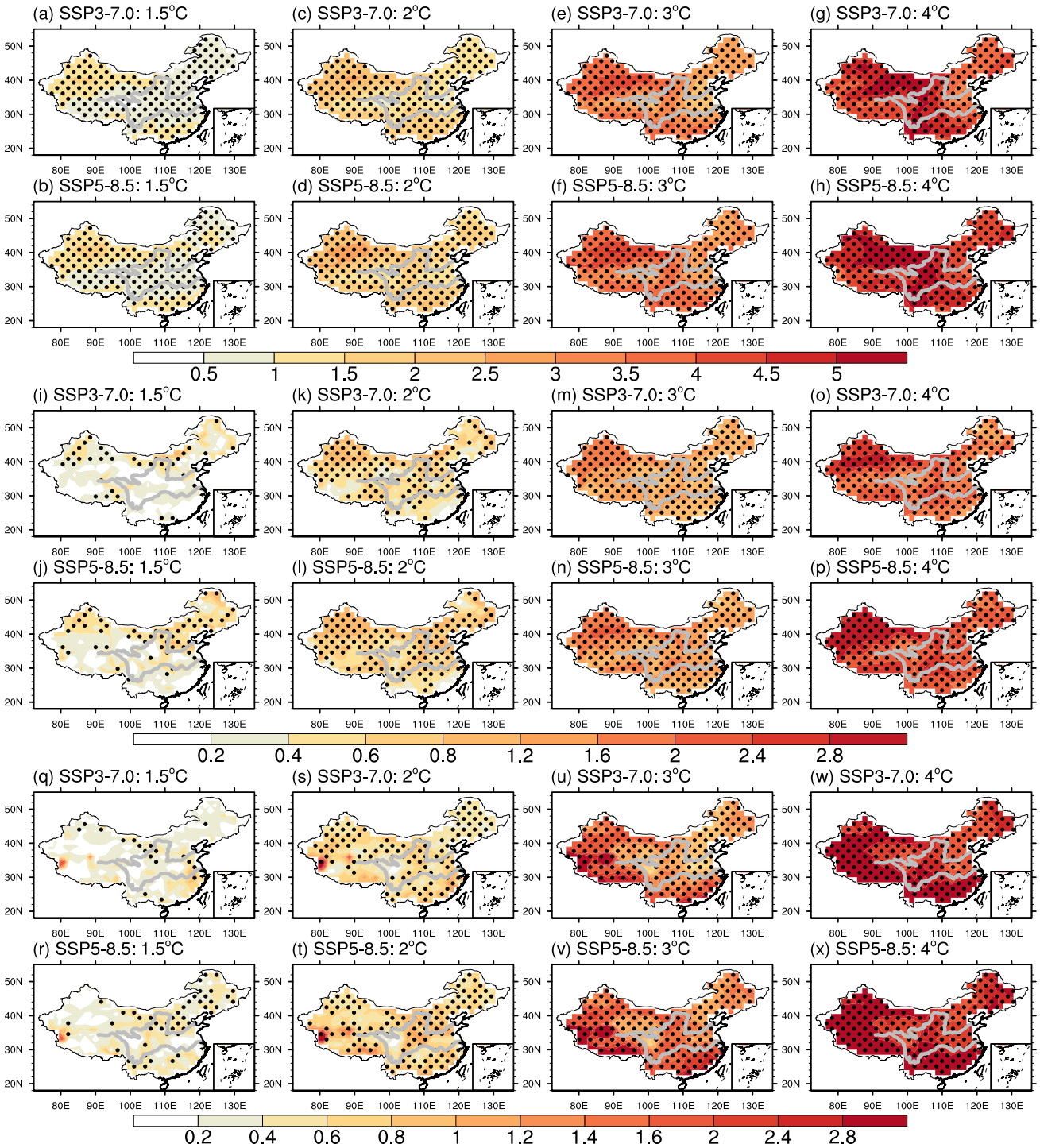

Fig. 4 The spatial patterns of changes in the frequency (**a**–**h**, units: events a^{-1}), intensity (**i**–**p**, units: ℃) and duration (**q**–**x**, units: days) of Compound HWs at 1.5 ℃ (2 ℃; 3 ℃; 4 ℃) GWL relative to the recent climate (1995–2014) under the two scenarios. Dots denote regions where at least 7 out of the 9 models agree on the sign of changes

and North China (NEC; 35°–54° N, 105°–134.5° E), Southeast China (SEC; 21°–35° N, 105°–123° E), Southwest China (SWC; 21°–37° N, 73°–105° E) and Northwest China (NWC; 37°–50° N, 73°–105° E). This study focuses on the changes during summer (June–August).

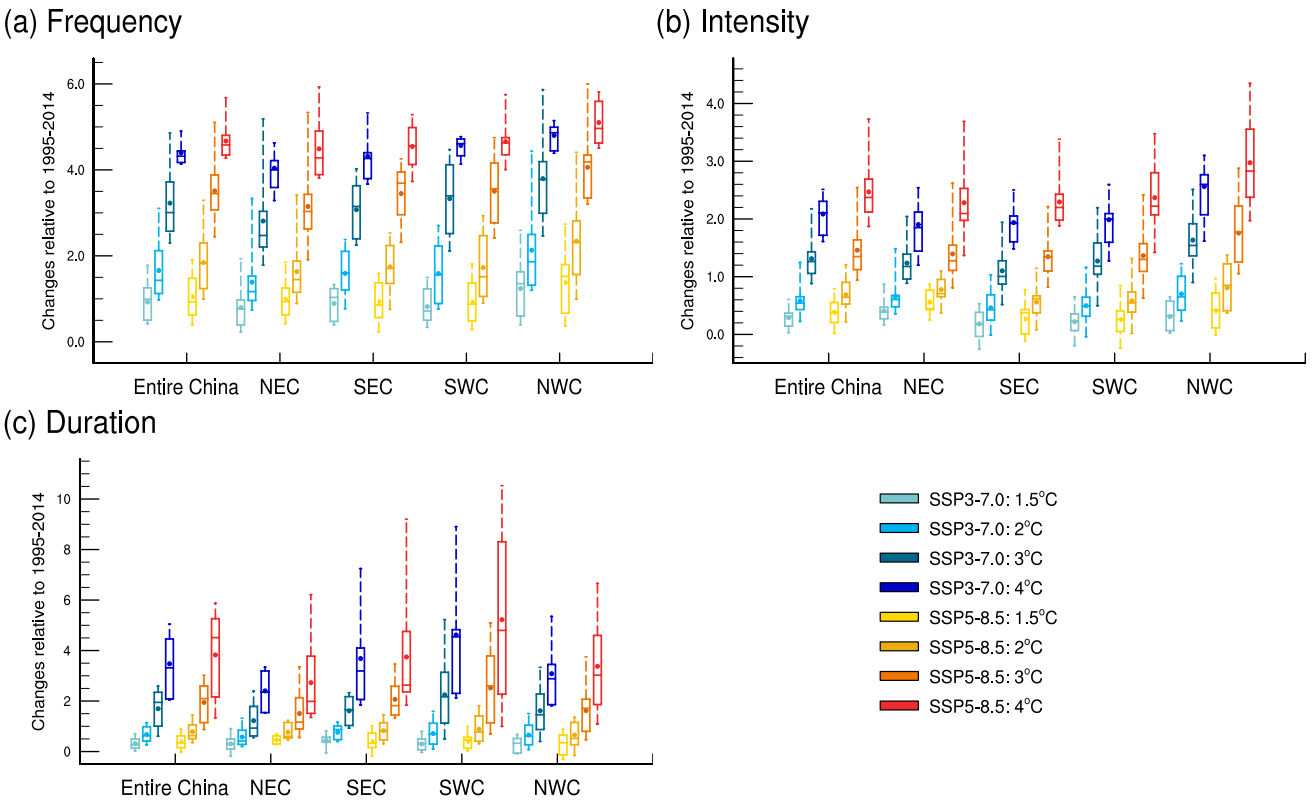

Fig. 5 Box plots of the regionally averaged changes in the frequency (**a**, units: events a^{-1}), intensity (**b**, units: ℃) and duration (**c**, units: days) of Compound HWs at 1.5 ℃ (2 ℃, 3 ℃, 4 ℃) GWL relative to the recent climate (1995–2014) under the two scenarios over the entire China and subregions. With each box, the horizontal lines from top to bottom denote the maximum value, the 75th percentile, the median value, the 25th percentile and the minimum value of the 9 models. The dot represents the multi-model ensemble mean whose sign agrees with at least 7 out of the 9 models

Table 2 The spatial pattern correlation coefficients of the future changes in frequency, intensity and duration of Compound HWs at different GWLs between the SSP3-7.0 and SSP5-8.5

	1.5 °C	2 °C	3 °C	4 °C
Frequency	0.91	0.96	0.95	0.87
Intensity	0.74	0.84	0.90	0.89
Duration	0.67	0.89	0.94	0.91

2.2 Methods

2.2.1 Definition of HWs

In order to define Compound HWs, a relative threshold on each calendar day is calculated as the daily 90th percentile of Tmax or Tmin based on 15-day window centered on that day during the baseline period of 1961–1990 (Della-Marta et al. 2007). Compound HWs are identified when the daily Tmax and Tmin exceed the baseline 90th percentile for at least three consecutive days.

Three features, that is frequency, intensity and duration, are used to characterize Compound HWs. The frequency is the accumulated number of Compound HW events within a year. The intensity of each event is calculated by averaging the daily Tmax and Tmin temperature anomalies above the corresponding thresholds within the event. The duration is the number of days from the beginning to the end of an event. The intensity and duration of events for a year are computed by averaging the intensity and duration of events occurring in that year. In addition, the max-duration event, which is used to present extreme long-lasting Compound HWs in a given year, is also analyzed.

2.2.2 Time windows of the 1.5 °C, 2 °C, 3 °C and 4 °C global warming levels

According to the IPCC AR6 report (Lee et al. 2021), 1850–1900 and 1995–2014 are defined as the pre-industrial period and the recent climate period, respectively. The global warming levels refer to the GMST under the two scenarios which is 1.5 °C, 2 °C, 3 °C and 4 °C higher than the GMST during the pre-industrial period. To reduce

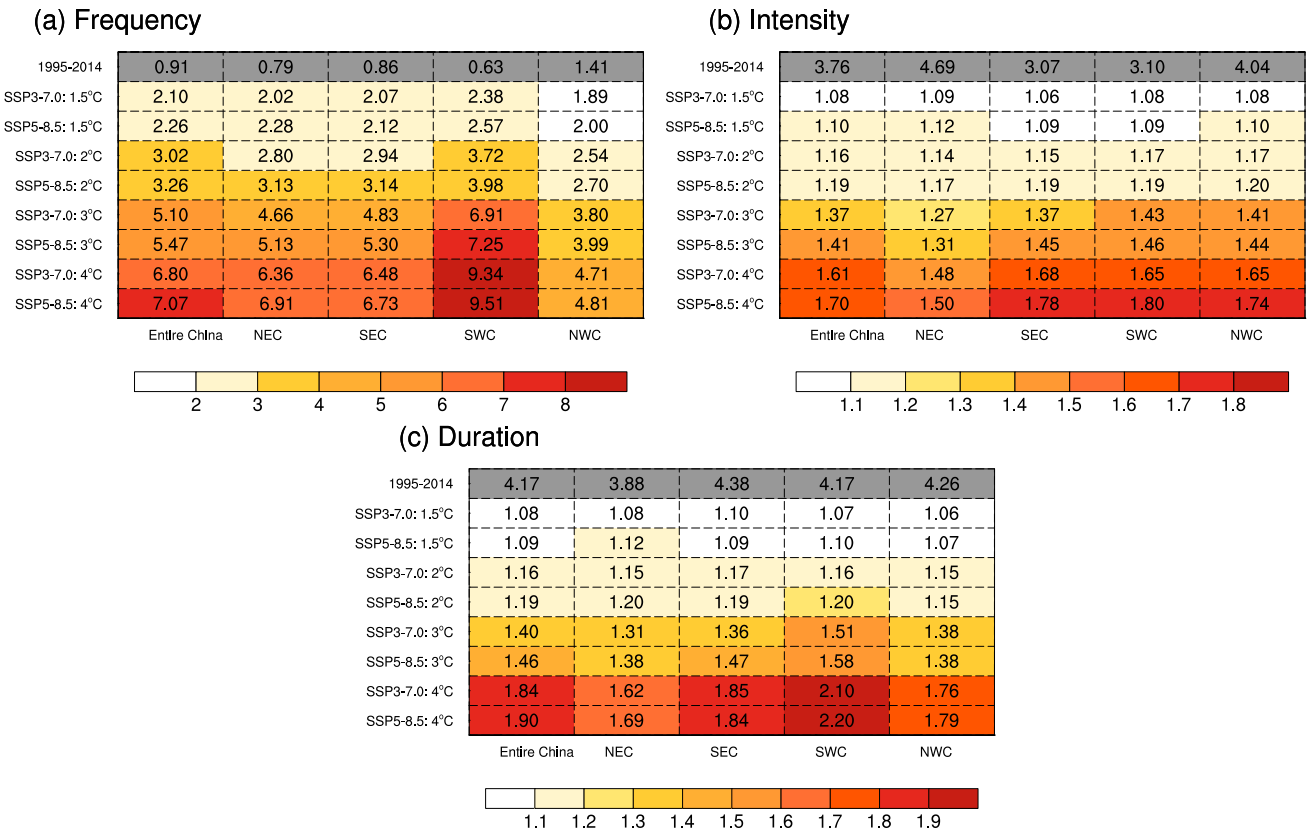

Fig. 6 The ratios relative to the recent climate (1995–2014) of frequency (**a**), intensity (**b**) and duration (**c**) of Compound HWs at the 1.5 ℃; 2 ℃; 3 ℃ and 4 ℃ GWLs under the two scenarios over the entire China and subregions. The first row in each panel is the regional averaged properties over the entire China and subregions in the recent climate (units are events•a^{-1}, ℃ and days, respectively)

the uncertainty in calculating the warming threshold-crossing times due to interannual variability, a 20-year running average is used to smooth the GMST time series (Liu et al. 2020). A 20-year window, which has 10 years before and 9 years after the year that exceeds the four global warming thresholds, is used to obtain relatively stabilized future climate states at different GWLs. Each member in CMIP6 model owns its individual time window of each GWLs. Figure 2 shows the GMST anomalies relative to the pre-industrial period. All members can reach 3 ℃ GWL under the two scenarios. All members under the SSP5-8.5 can reach the 4 °C GWL by the end of the 21st century, but only 14 members (6 models) can reach this target under the SSP3-7.0. The differences of HWs properties between different GWLs and the recent climate are regarded as the future changes of HWs (Domeisen et al. 2023). Consistence among models is performed by at least 7 out of 9 models agreeing on the sign of multi-model ensemble mean changes.

2.2.3 Probability ratios of compound HWs

The probability ratio (PR) is defined as the ratio of the probability of Compound HWs at different GWLs to the probability in the recent climate (Sun et al. 2018) and this ratio quantifies the changing probability of an event in future relative to present climate. The extreme Compound HWs are events with a 50-year or 100-year return periods in the recent climate. The thresholds of these two relatively rare extreme events are obtained by Gumbel extreme value distribution function which is helpful to identify the temporal distribution of meteorological extreme values with various return periods (Gumbel 1942; Zhou et al. 2009; Yao et al. 2018). Therefore, PR for these extreme rare events is calculated by P_1/P_0, in which P_1 is the probability of 50-year (100-year) events at different GWLs and P_0 is 2% (1%) for 50-year (100-year) events in the recent climate.

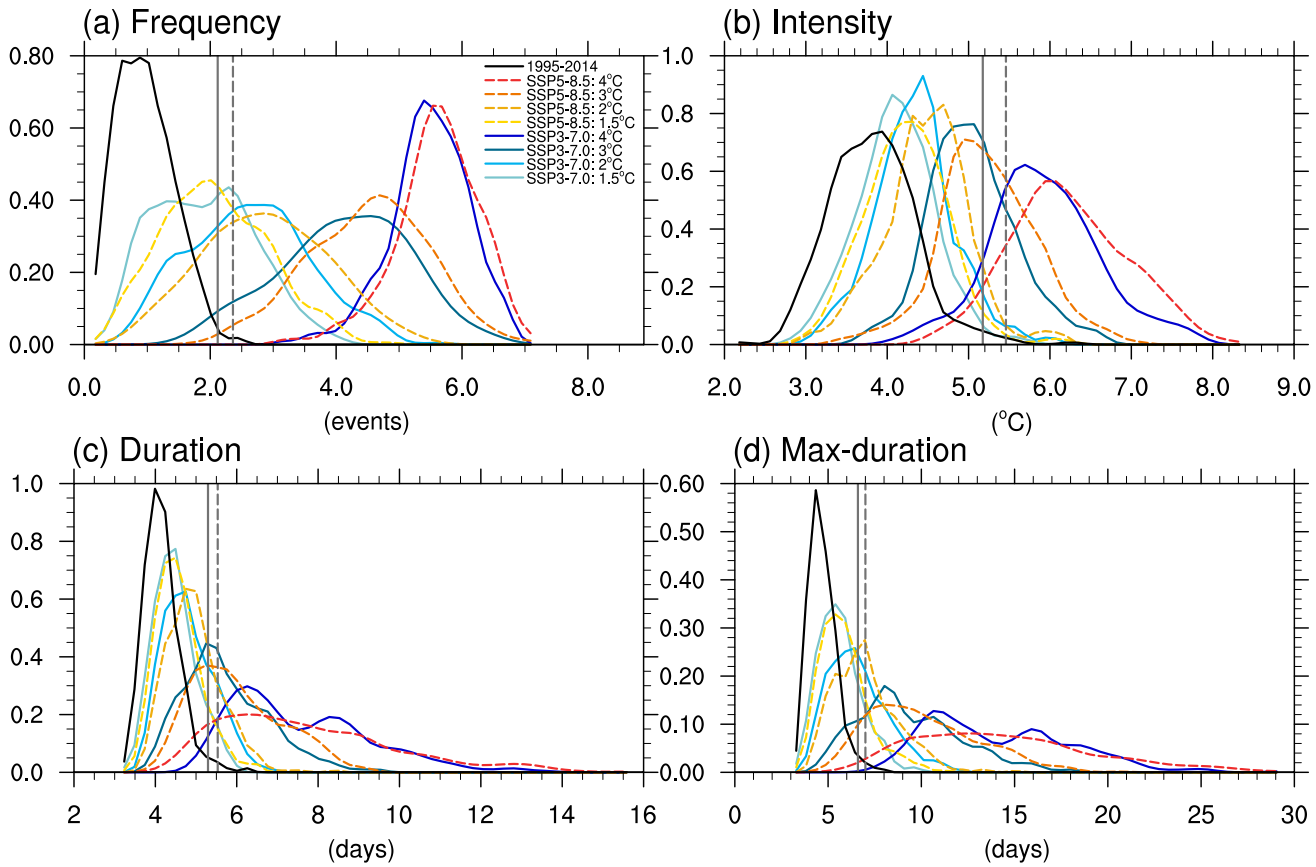

Fig. 7 The Kernel probability density functions (PDFs) of frequency (**a**), intensity (**b**), duration (**c**) and max-duration (**d**) of Compound HWs over the entire China in the recent climate (black), 1.5 ℃, 2 ℃, 3 ℃ and 4 ℃ GWLs. Solid (Dashed) lines represent SSP 3–7.0 (SSP5-8.5). Grey solid (dashed) line represents the threshold of 50-year (100-year) event based on the recent climate of 1995–2014

3 Projected changes of compound HWs properties

3.1 The changes of compound HWs at different global warming levels

The models chosen for this study represent some main characteristics and spatial variations of Compound HWs in terms of frequency, intensity and duration during the historical period (Supplementary Fig. S1). The multi-model ensemble mean captures the locations of high value centers of the three properties across China, especially over the eastern part of China. The pattern correlation coefficient of intensity between model simulations and observations can reach 0.90. However, the correlation coefficient of frequency and duration is only about 0.21 and 0.06, respectively. These low correlations suggest that model have some biases in simulating climatological spatial distributions of frequency and duration. To show if model can capture observed changes during the historical period, the linear trends of Compound HW properties during the period 1961–2020 in observations and model simulations over various regions are analyzed and results are given in Supplementary Fig. S2. Although there are biases over the western China with HW properties underestimated by 20–25% in model simulations, the model can well reproduce the observed trends over the other regions. Furthermore, the multi-model mean of CMIP6 can well represent the historical temperature distributions over China with pattern correlation coefficients over 0.95 (Supplementary Fig. S3). The differences between model simulations and observations show relatively large biases over the western China than the other regions, with cold biases being associated with underestimated trends of HW properties. Although the biases might affect the model simulated HWs over the western China, the models can capture the main features of observed trends of HWs during the historical period, giving the fidelity using such models to assess future changes.

The spatial patterns of frequency, intensity and duration of the Compound HWs in the recent climate and at different GWLs are shown in Fig. 3 and the future changes in these properties are given in Fig. 4, respectively. The largest frequency of Compound HWs appears over Northwest China with a value of 1.76 events per year (hereafter as events

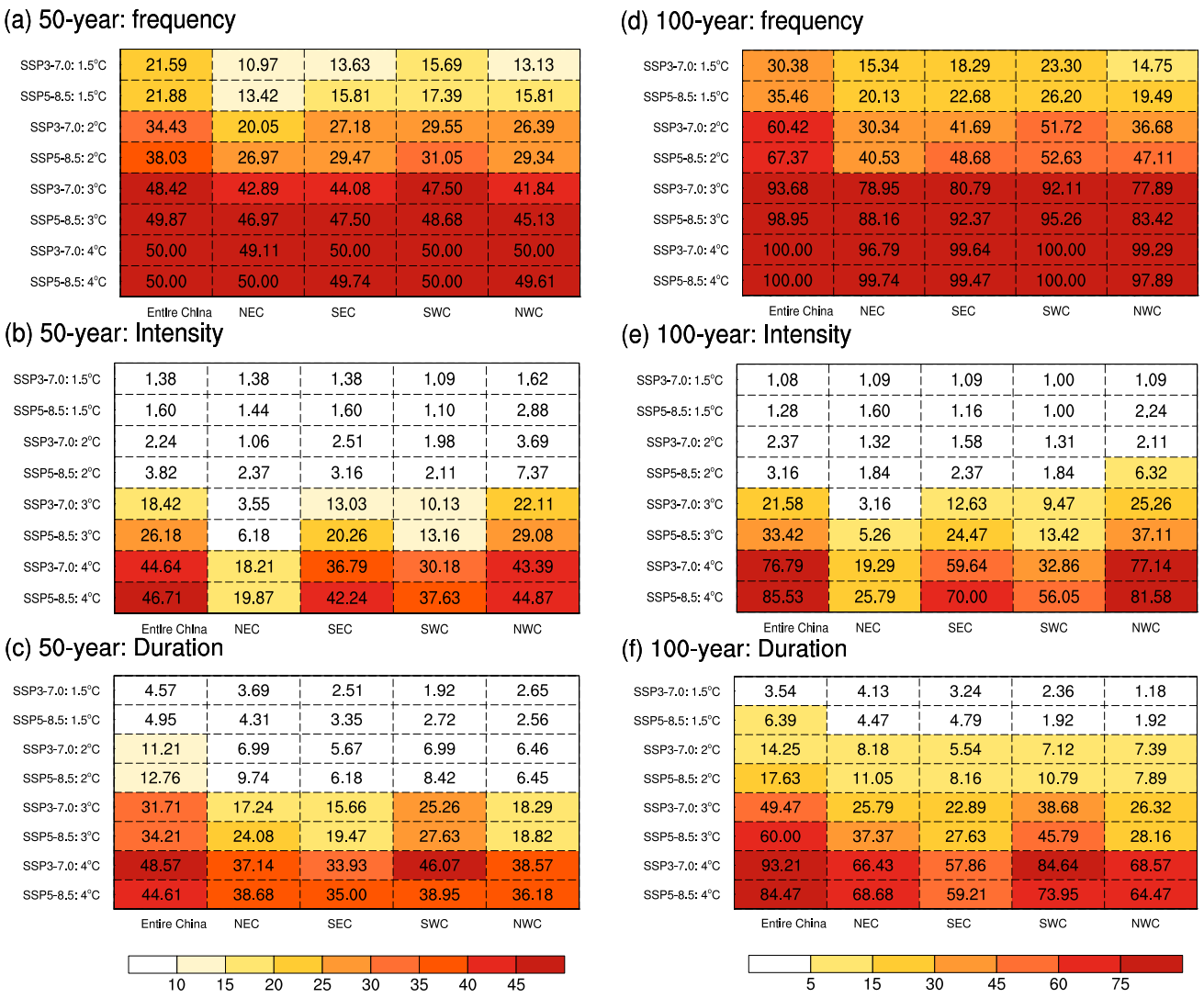

Fig. 8 The probability ratios of frequency, intensity and duration of a 50-year (**a**–**c**) and 100-year (**d**–**f**) Compound HWs at the 1.5 ℃; 2 ℃; 3 ℃ and 4 ℃ GWLs relative to the recent climate (1995–2014) under the two scenarios over the entire China and subregions

a^{-1}) in the recent climate. With the increasing of GMST, the largest frequency of Compound HWs is much larger, with a value of 3.57 (4.37; 6.13; 7.11) events a^{-1} at the 1.5 ℃ (2 ℃; 3 ℃; 4 ℃) GWL. In terms of future changes, the frequency of Compound HWs increases significantly over the entire China, especially over Northwest China and Southeast China with a maximum increase of 1.71 (2.74; 4.45; 5.81) events a^{-1} at the 1.5 ℃ (2 ℃; 3 ℃; 4 ℃) GWL (Fig. 4a–h).

The magnitude of intensity of Compound HWs increases from south to north with a range of 1.17–6.50 ℃ in the recent climate. However, the intensity increases with increasing GWL. Specifically, the range of Compound HWs intensity is 1.50–6.36 (1.79–6.61; 2.66–7.17; 3.61–8.31) ℃ over China at the 1.5 ℃ (2 ℃; 3 ℃; 4 ℃) GWL. The largest future changes of intensity occur over the Northwest China, with an increase by 0.72 (1.06; 2.11; 3.46) ℃ at the 1.5 ℃ (2 ℃; 3 ℃; 4 ℃) GWL (Fig. 4i–p). Particularly, the enhancements of intensity among models become more consistent over the entire China above the GWL of 3℃.

For duration, the Compound HWs last longer over western China and Southeast China with a maximum duration of 5.87 days in the recent climate. However, the duration is prolonged with increasing GWLs, with the maximum duration of 7.85 (9.75; 15.71 and 26.79) days at the 1.5 ℃ (2 ℃; 3 ℃; 4 ℃) GWL. The regional differences of the future changes at the 1.5 ℃ and 2 ℃ GWLs are relatively small compared with the 3 ℃ and 4 ℃ GWLs (Fig. 4q–x). At the 3 ℃ (4 ℃) GWL, the duration increases significantly over the entire China and the largest changes appear over Southeast China with a value of 10.27 (21.28) days.

The regionally averaged changes of Compound HWs properties over the entire China and subregions are shown

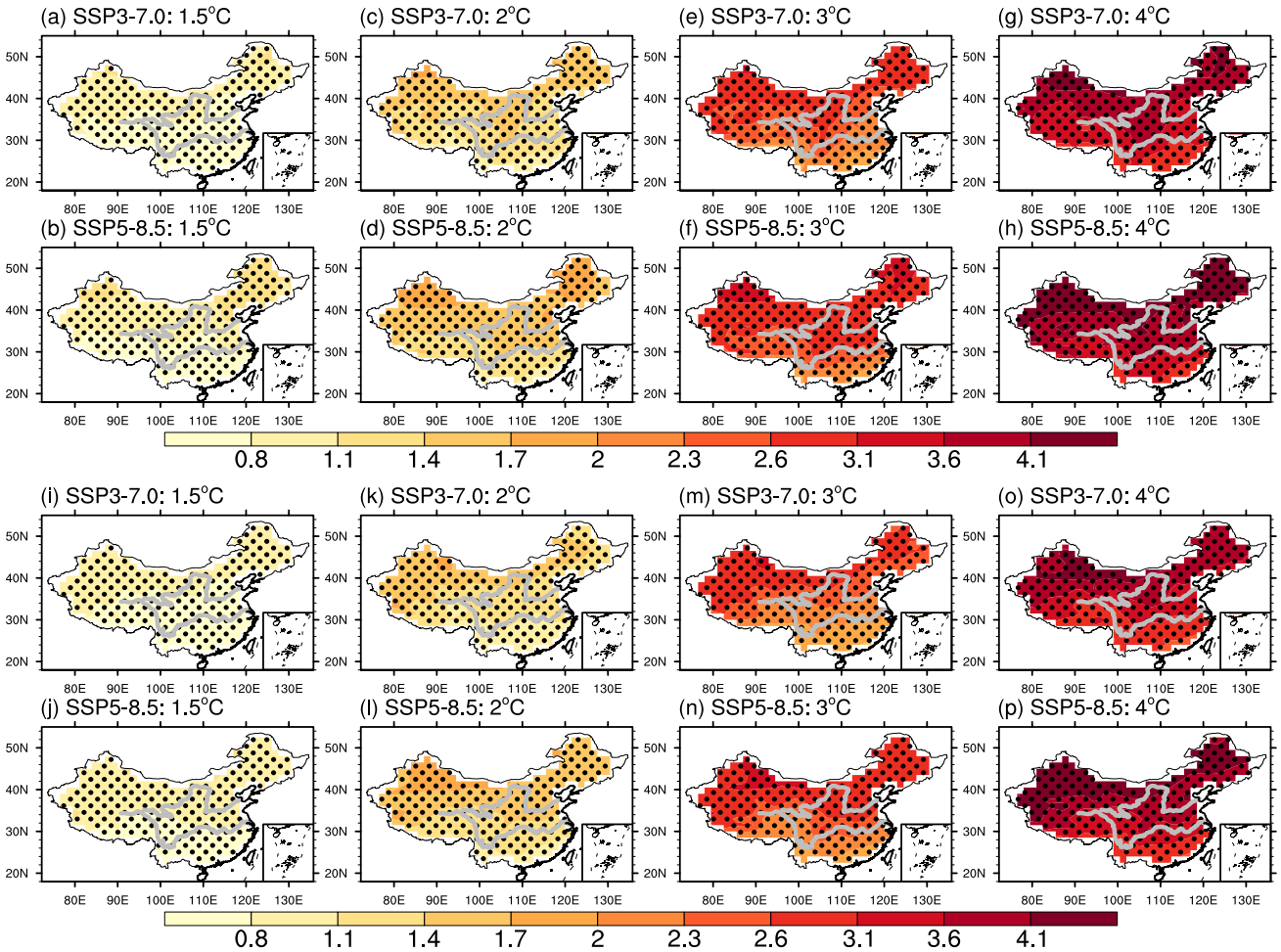

Fig. 9 The spatial patterns of changes in summer mean Tmax (**a**–**h**, units: ℃) and Tmin (**i**–**p**, units: ℃) at 1.5 ℃ (2 ℃; 3 ℃; 4 ℃) GWL relative to the recent climate (1995–2014) under the two scenarios. Dots denote regions where at least 7 out of the 9 models agree on the sign of changes

in Fig. 5. The frequency over the entire China increases by about 0.99 (1.75; 3.37; 4.53) events a^{-1} at the 1.5 ℃ (2 ℃; 3 ℃; 4 ℃) GWL compared with the recent climate (Fig. 5a). The largest change of regional averaged frequency appears over NWC with a range of 1.31–4.95 events a^{-1}. The intensity of Compound HWs intensifies significantly over the entire China (0.34; 0.63; 1.39; 2.28 ℃). However, the intensification over NEC and NWC is larger than the other subregions. SEC shows the smallest intensification of 0.23–2.12 ℃ (Fig. 5b). In terms of duration, Compound HWs last longer over the entire China by 0.35 (0.73; 1.82; 3.65) days at the 1.5 ℃ (2 ℃; 3 ℃; 4 ℃) GWL relative to the recent climate, especially over SWC with a value of 4.92 days at the 4 ℃ GWL (Fig. 5c). The increase of duration over NWC is the weakest among all subregions. It can be seen that the amplifications in these three properties increase with the GWLs over the entire China and subregions. However, the future changes in Compound HWs vary nonlinearly with the GWLs (Supplementary Fig. S4). For example, the increase in the frequency of HWs is smaller when moving from the 3 ℃ to 4 ℃ GWL compared to the 1.5 ℃ to 3 ℃ GWL, which is related with the increased changing rate of duration. More short duration HWs change to long duration HWs, leading to the decreased changing rate of frequency. The changing rate of intensity is almost linear which is related to the linear variation of surface air temperature with GWLs. Furthermore, in some boxes of Fig. 5, there is a large spread among the models. For frequency, this spread is the smallest at the 4 ℃ GWL compared with the other GWLs. However, for duration, the model spread increases with increasing GWL.

Although there is considerable sensitivity in the properties of Compound HWs to the GWLs, we do not find a large sensitivity to the emissions scenario. That is, the spatial patterns of changes in the frequency, intensity and duration of Compound HWs at different GWLs are similar under the SSP3-7.0 and SSP5-8.5. Table 2 provides the spatial pattern

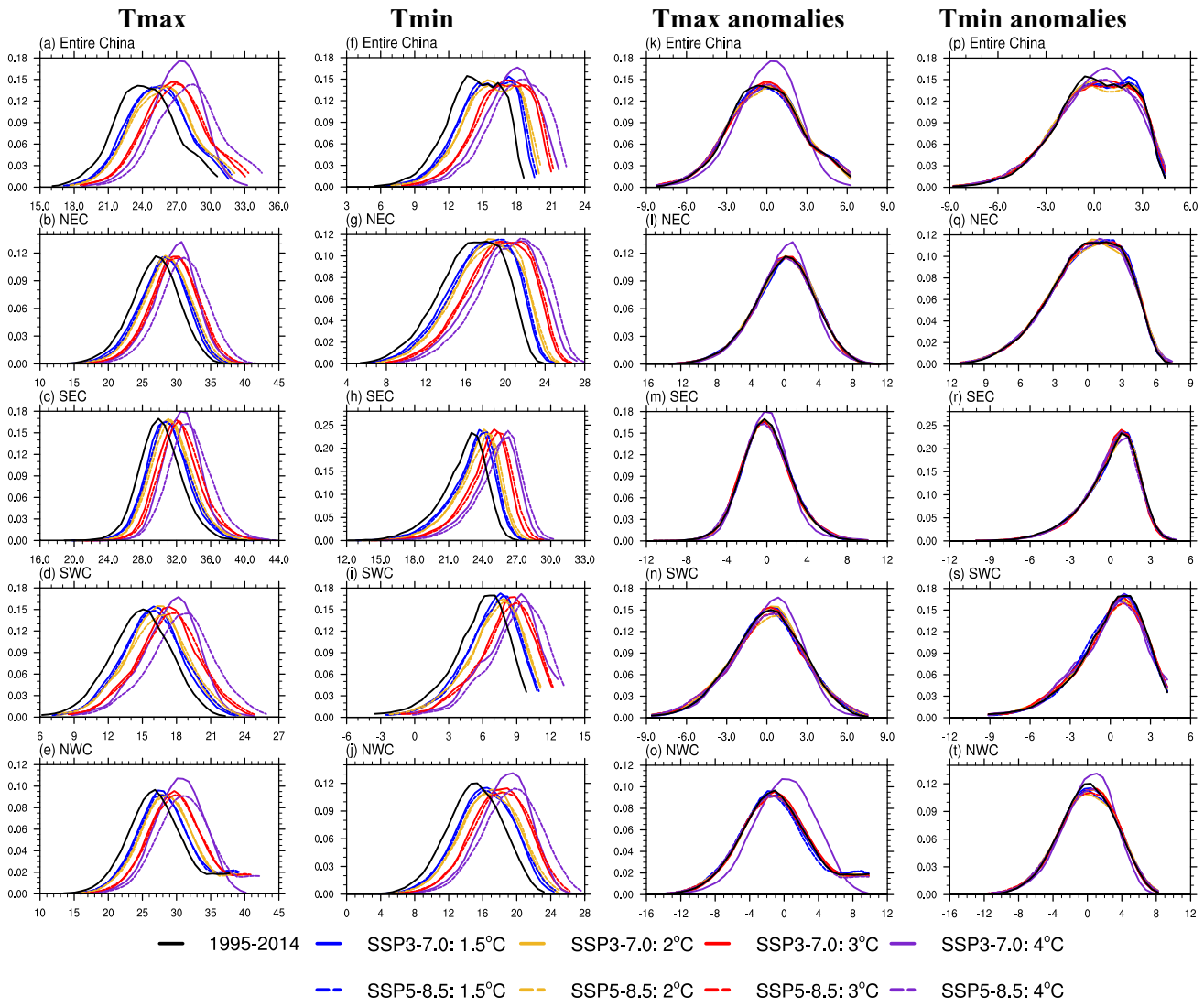

Fig. 10 The Kernel probability density functions of daily Tmax (**a**–**e**), daily Tmin (**f**–**j**), daily Tmax anomalies (**k**–**o**) and daily Tmin anomalies (**p**–**t**) relative to corresponding mean Tmax and Tmin in each GWLs averaged over the entire China and the four subregions

correlations between SSP3-7.0 and SSP5-8.5 of the future changes and they show high correlations of about 0.67–0.96. These high spatial pattern correlations, together with similar magnitudes of HW properties changes (Figs. 4 and 5) indicate that the future changes of Compound HWs are primarily determined by the GWLs and are not very sensitive to the scenarios.

Figure 6 further illustrates the changes in properties of Compound HWs by showing the ratios of future changes relative to the recent climate at different GWLs. The ratios of frequency are much larger than the other two properties, which can reach 2.26 (3.26; 5.47; 7.07) times of the frequency during the recent climate at the 1.5 ℃ (2 ℃; 3 ℃; 4 ℃) GWL over the entire China under the SSP5-8.5. From 1.5 to 4 ℃ GWL, the frequency increases by about 3.5 times. For intensity and duration, the ratios at the four GWLs over the entire China are around 1.08–1.90 times of those during the recent climate. SWC exhibits the largest ratios with a range of 2.38–9.51 (1.08–1.80; 1.07–2.20) in frequency (intensity; duration). These ratios mean that the frequency can reach 1.50–6.00 events a^{-1} at different GWLs in comparison with 0.63 events a^{-1} in the recent climate. The intensity will be 3.35–5.58 ℃ hotter and duration will be 4.46–9.17 days longer at different GWLs in the future climate in comparison with those in the recent climate.

3.2 The probability ratios of extreme Compound HWs

Figure 7 shows the probability density functions (PDFs) of Compound HWs over the entire China in the recent climate

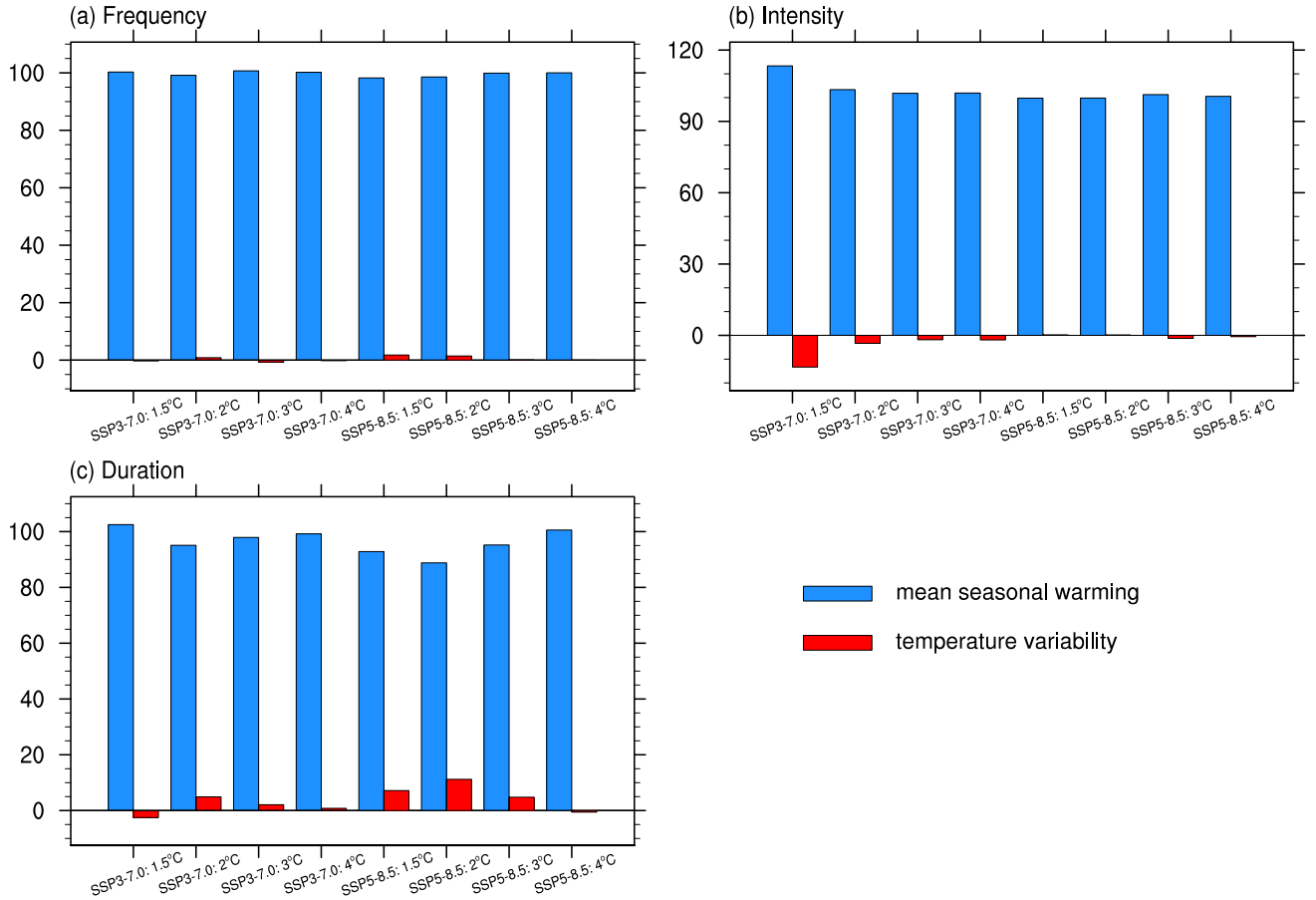

Fig. 11 The contributions of seasonal mean warming (blue bar) and changes in temperature variability (red bar) to the future changes of frequency (**a**), intensity (**b**) and duration (**c**) of Compound HWs averaged over the entire China at different GWLs (units: %)

and different GWLs. The PDFs of the four HW properties at different GWLs shift rightward from the recent climate with the largest shift seen at the 4℃ GWL. These shifts indicate both means of HW properties and extreme rare HW events increase with increasing GWL. Heatwave events become more frequent and the temperatures of each event become hotter at different GWLs than those in the recent climate (Fig. 7a and b). For duration (Fig. 7c and d), the shapes of PDFs at different GWLs become more flattened and right-skewed than the shape in the recent climate, which indicate large increases in extreme long duration events at the four GWLs. Compared with the other three GWLs, the duration becomes much longer at the 4℃ GWL (Fig. 7c). The longer duration can constrain the increase of frequency, leading to the weak frequency variance at the 4℃ GWL (Fig. 7a). The shapes of the PDFs for max-duration are similar to PDFs shapes of mean duration. In particular, Fig. 7d shows that the duration of extreme long-lasting Compound HWs at the 4℃ GWL can reach more than 25 days in summer in comparison with 8 days in the recent climate. In contrast to the PDFs of frequency and duration, the PDFs of intensity show that changes are dominated by a rightward shift with little change in shape for increasing GWLs in comparison with the one in recent climate (Fig. 7b). For the most intense events which occur at the 4℃ GWL, the variance of intensity increases compared with the recent climate. Supplementary Figure S5 shows the regional averaged PDFs over the four subregions. The main features in changes of PDFs for intensity, duration and max-duration over subregions are similar to the features of changes over the entire China.

To illustrate how the extremely rare HW events will change at different GWLs, the grey lines in Fig. 7 show the thresholds of 50-year and 100-year events based on the recent climate. The probabilities of these two kinds of extremely rare events increase significantly with increasing GWLs and they will become much more frequent in the future. Furthermore, the quantitative analysis about probability ratios of these two extreme Compound HWs over different regions is summarized in Fig. 8. In particular, the PRs for frequency (Fig. 8a, d) are much larger than the PRs of intensity and duration. However, the regional differences in the PRs are not obvious among the subregions.

The PRs of the two extreme rare events increase gradually with the increasing of GWLs. Especially, the PRs are close to 50 (100) for the 50-year (100-year) event at the 4 ℃ GWL, which indicates these two kinds of extreme rare events will become 1-year events. For intensity (Fig. 8b, e), the probabilities of the two extreme rare events show weak changes at the 1.5 ℃ and 2 ℃ GWLs relative to the recent climate. At the 3 ℃ and 4 ℃ GWLs, NWC exhibits the largest PRs with a value of 29.08 and 44.87 (37.11 and 81.58) for the 50-year (100-year) event, so that the 50-year (100-year) event in the recent climate will become a 1.7-year and 1.1-year (2.7-year and 1.2-year) event in the future. From the 1.5 ℃ to 4 ℃ GWL, the PRs of duration of 50-year (100-year) event over the entire China increase from 4.57 (3.54) to 48.57 (93.21) (Fig. 8c, f). The PRs of duration over SWC are the largest among the subregions. At the 4℃ GWL, the 50-year and 100-year events over SWC will become 1-year and 1.2-year events, respectively.

In summary, the analyses about HW properties change at different GWLs suggest that HWs over China become more frequent, event temperature becomes hotter, and event duration becomes longer at different GWLs than those in the recent climate. The magnitudes of these changes depend on GWLs but they are not very sensitive to scenarios. Specifically, at the 4 ℃ GWL, the frequency of HWs increases by more than fivefold under both scenarios, and the intensity (duration) of HWs averaged under the two scenarios is 2.28 ℃ hotter (3.59 days longer) than the one in the recent climate over the entire China. Furthermore, the maximum duration of HW events can reach more than 25 days in summer at 4 ℃ GWL in comparison with 8 days in the recent climate. The extreme rare events (50-year and 100-year events) in the recent climate would become the norm over China and four sub-regions at 4 ℃ GWL.

4 The responsible physical processes related to the changes of compound HWs properties

4.1 The roles of seasonal mean temperature and temperature variability changes on HW property changes

Future changes in the properties of HWs in global warming worlds can be contributed by the changes in the climatological seasonal mean temperature and the changes in temperature variability (Argueso et al. 2016; Su and Dong 2019a). Figure 9 shows the future changes of summer mean Tmax and Tmin at different GWLs relative to the recent climate. Overall, the spatial patterns of the temperature change are similar at the four GWLs. However, the future changes of seasonal mean temperature do show significant regional differences. In particular, the magnitude of temperature change increases from south to north and the largest increase at each GWL appears over Northwest China, which is consistent with the larger increase of future changes in frequency and intensity of HWs over the northern part of China.

Figure 10 shows the PDFs of daily Tmax and Tmin averaged over the entire China and the four subregions. The PDF shapes of Tmax and Tmin at different GWLs and recent climate have similar distribution patterns except a shift to increasing temperatures with increasing GWL. After removing the corresponding local mean temperature at the different GWLs, the distributions of daily temperature anomalies at different GWLs are very similar. Therefore, the Tmax and Tmin at different GWLs have similar daily to sub-seasonal time scale variability. However, the PDFs of Tmax anomalies at the 4 ℃ GWL under the SSP3-7.0 do show some differences from other PDFs (Fig. 10k–o), but this may be due to the fact that only 6 models can reach the 4℃ GWL under this scenario compared with 9 models at other GWLs. Supplementary Figure S6 illustrates the PDFs of Tmax anomalies with the same model members at the four GWLs and they show very similar distributions, suggesting that slightly different PDF distributions at the 4 ℃ GWL under the SSP3-7.0 in comparisons with those in other GWLs shown in Fig. 10 are mainly due to less model members reaching 4 ℃ GWL under this scenario.

To further assess the roles of seasonal mean temperature changes and temperature variability changes on HW property changes, reconstructed Tmax and Tmin time series for each GWL are made by adding the summer climatological mean Tmax and Tmin differences between two periods (GWL minus the recent climate) to the original daily Tmax and Tmin time series during the recent climate. In this way, the reconstructed time series at each GWL have the same temperature variability as the original time series during the recent climate but with the seasonal mean warming added. Therefore, any difference in Compound HW properties between the reconstructed time series at each GWL and the time series during the recent climate are due to the seasonal mean warming signal. In contrast, the differences in Compound HW properties between the original time series for future climate and reconstructed time series are due to temperature variability. Figure 11 shows that the role of the seasonal mean warming dominates the changes in the HW properties at the different GWLs over the entire China, especially for increases in frequency. For each subregion, the seasonal mean warming also plays a dominant role on the changes in the HW properties (Supplementary Fig. S7). The importance of seasonal mean warming is consistent with the previous studies that the seasonal mean temperature changes control future HWs across the world and in different regions

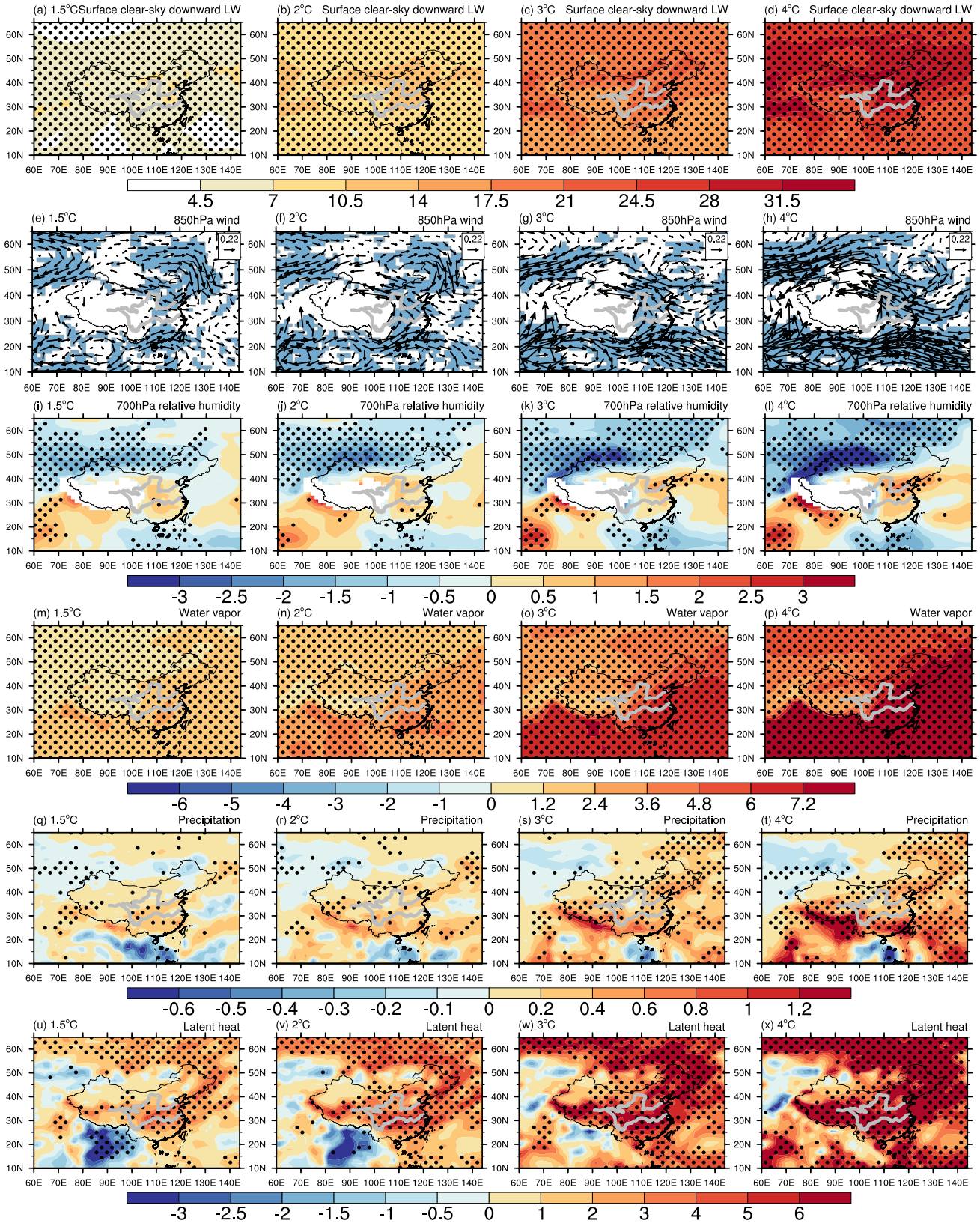
(a) 1.5°CSurface clear-sky downward LW
(b) 2°C Surface clear-sky downward LW
(c) 3°C Surface clear-sky downward LW
(d) 4°C Surface clear-sky downward LW
4.5 7 10.5 14 17.5 21 24.5 28 31.5
(e) 1.5°C 850hPa wind
(f) 2°C 850hPa wind
(g) 3°C 850hPa wind
(h) 4°C 850hPa wind
(i) 1.5°C 700hPa relative humidity
(j) 2°C 700hPa relative humidity
(k) 3°C 700hPa relative humidity
(l) 4°C 700hPa relative humidity
-3 -2.5 -2 -1.5 -1 -0.5 0 0.5 1 1.5 2 2.5 3
(m) 1.5°C Water vapor
(n) 2°C Water vapor
(o) 3°C Water vapor
(p) 4°C Water vapor
-6 -5 -4 -3 -2 -1 0 1.2 2.4 3.6 4.8 6 7.2
(q) 1.5°C Precipitation
(r) 2°C Precipitation
(s) 3°C Precipitation
(t) 4°C Precipitation
-0.6 -0.5 -0.4 -0.3 -0.2 -0.1 0 0.2 0.4 0.6 0.8 1 1.2
(u) 1.5°C Latent heat
(v) 2°C Latent heat
(w) 3°C Latent heat
(x) 4°C Latent heat
-3 -2.5 -2 -1.5 -1 -0.5 0 1 2 3 4 5 6

◂**Fig. 12** Spatial distributions of the changes in surface clear-sky downward longwave radiation (**a**–d, units: W m^{-2}), 850 hPa wind (**e**–**h**, vector, units: m s^{-1}), 700 hPa relative humidity (**i**–**l**, units: %), water vapor (**m**–**p**, units: kg m^{-2}), precipitation (**q**–**t**, units: mm day^{-1}), and latent heat (**u**–**x**, units: W m^{-2}, positive values mean upward) at 1.5 ℃ (2 ℃; 3 ℃; 4 ℃) GWL under the SSP5-8.5 relative to the recent climate. Shading in **e**–**h** and dots in **a**–**d**; **i**–**x** denote regions where at least 7 out of the 9 models agree in the sign of changes

(Argueso et al. 2016; Su and Dong 2019a; Zhao et al. 2019). Therefore, it's reasonable to analyze the changes of physical variables in climatological seasonal mean state between different GWLs and the recent climate to discuss the responsible physical processes. Due to the difference in radiative forcing between the SSP5-8.5 and SSP3-7.0, the physical processes of these two scenarios will be analyzed separately.

4.2 The physical processes under the SSP5-8.5

Figure 12 shows seasonal mean changes in some key variables at different GWLs relative to the recent climate. The surface clear-sky downward longwave radiation increases significantly over China, with large increases over NWC and eastern China (Fig. 12a–d). The magnitudes of changes increase with increasing GWLs. These increases are likely to be partly due to the increase in greenhouse gas forcing and partly due to the increase of water vapor in the atmosphere related to warming (Fig. 12m–p). The southwesterly wind anomalies over SEC and the anomalous moist air flow from the Pacific Ocean (Fig. 12e–h) lead to increased moisture transport over eastern China, and is likely responsible for large increases in water vapor and increase in relative humidity there (Fig. 12i–l). The anomalous wind along the east periphery of the Tibetan Plateau will also transport water vapor to NWC (Fig. 12m–p). The increases in clear sky downward longwave radiation tend to warm the surface. As the temperature differences between the surface and atmosphere increase, upward sensible heat fluxes from the surface to the atmosphere will also increase. The increased water vapor is also associated with increasing precipitation across China (Fig. 12q–t). The increased precipitation is beneficial for the increases of soil moisture through a positive feedback, since the water added to the land surface during rainfall leads to increased evaporation and this can lead to further precipitation in return (Douville et al. 2001; Sehler et al. 2019). Influenced by the strong controlling of soil moisture on evapotranspiration, the increased soil moisture contributes to the increase of water vapor in the atmosphere, which absorbs both shortwave and longwave radiation. (Fig. 12u–x, Xu et al. 2019). Due to the condensation during a precipitation event, the latent heat is released from water vapor and therefore transfers from the surface to the atmosphere. The increased upward sensible heat fluxes and the release of positive latent heat are beneficial for the warming of air temperature (Song et al. 2022). Hence, the increased heat fluxes are responsible for the stronger, longer and more frequent Compound HWs over China in the future climate.

The spatial patterns of some variables related to changes of aerosol forcing are illustrated in Fig. 13. At the 2 ℃; 3 ℃ and 4 ℃ GWLs, the aerosol optical depth (AOD) at 550nm decreases significantly over eastern China (Fig. 13c, d). However, due to the relatively weak changes of aerosol emission at the 1.5℃ GWL compared with the recent climate, there is a large spread in AOD at 550nm across models and there are even positive changes over the NEC (Fig. 13a). Influenced by aerosol-radiation interactions (Hatzianastassiou et al. 2007; Boucher et al. 2013), the decrease of AOD at 550nm results in the increase of net surface clear-sky shortwave radiation (Fig. 13e–h), which will also tend to warm the surface over eastern China. Larger changes in net surface shortwave radiation than clear sky shortwave radiation over eastern China indicate that part of surface shortwave radiation changes is related to an increased shortwave cloud radiative effect (Fig. 13i–l), induced by decreases in total cloud cover (Fig.13m–p), related to aerosol-cloud interactions (Boucher et al. 2013). These increases in net surface shortwave radiation also make contributions to the surface warming.

Considering the regional differences in HWs properties changes, the large increases in frequency and intensity of Compound HWs over the NWC are consistent with large increases in Tmin in the region (Fig. 9), which is likely related to the large increases in longwave radiation. Therefore, increases in both shortwave and longwave radiation appear responsible for increases in Tmax and Tmin over eastern China, leading to larger increases in frequency over the SEC and intensity over the NEC. Duration changes show large increases in SWC and SEC where model climatology also show long duration of Compound HWs, suggesting that duration changes might depend on the model climatology.

In summary, the surface warming across China seen in summer in the future climate is related to an increase in longwave radiation, partly resulted from the increase in greenhouse gas forcing and partly resulted from increased water vapor, and an increase in shortwave radiation over eastern China related to decreases in aerosols. The regional variations in the water vapor over China are consistent with atmospheric circulation changes. These seasonal mean surface warming results in enhanced upward sensible and latent heat fluxes, consistent with increased summer mean Tmax and Tmin and the enhancement of Compound HWs properties over China. Moreover, with the increasing of GWL, the magnitudes of the changes increase, which indicates that the influence of these processes on Compound HWs intensifies.

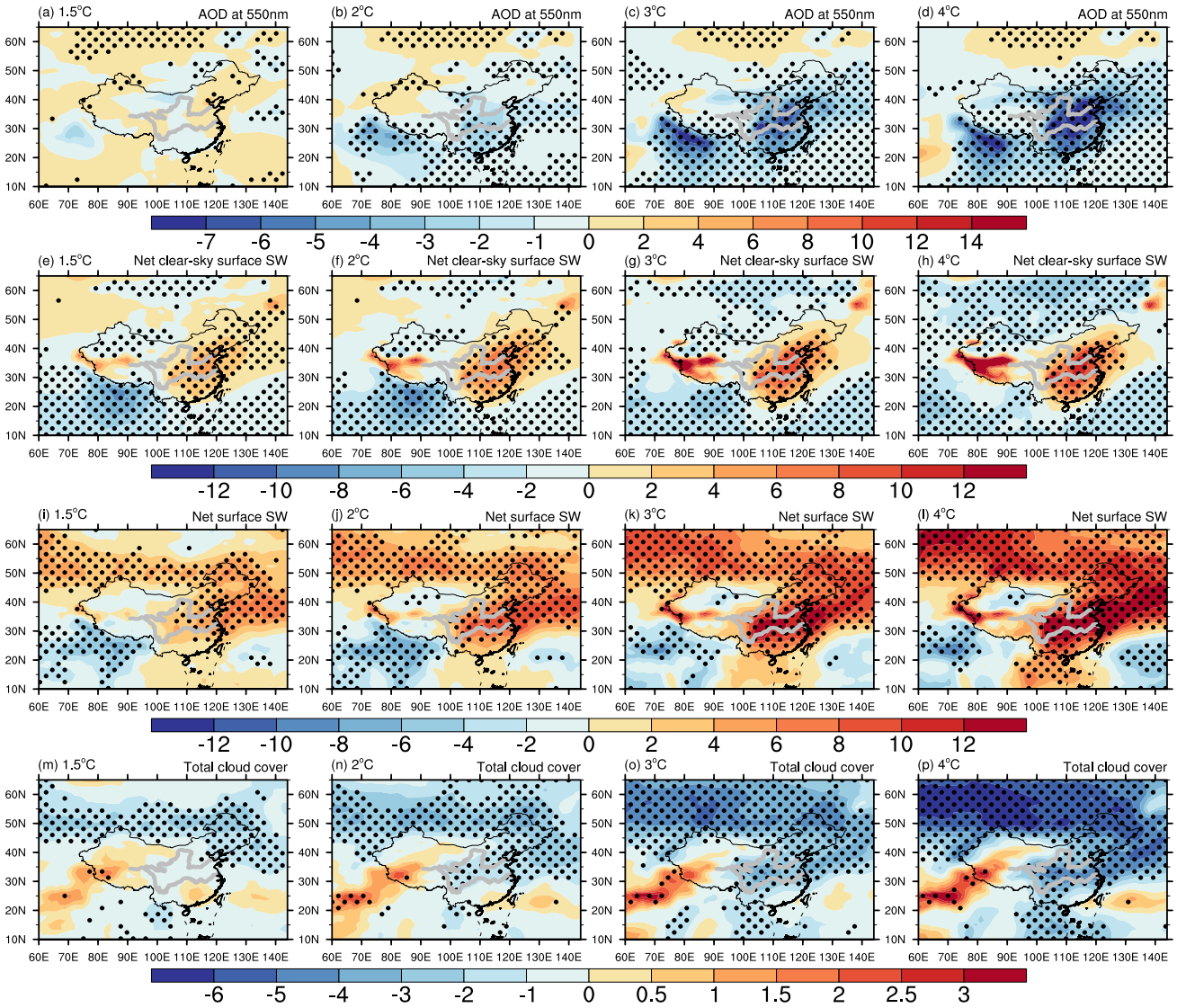

Fig. 13 Spatial distributions of the changes in aerosol optical depth (AOD) at 550 nm (**a**–**d**, units: 10^{-3}, results are based on 5 models in which AOD is available), net clear-sky surface shortwave radiation (**e**–**h**, units: W m^{-2}), net surface shortwave radiation (**i**–**l**, units: W m^{-2}), and total cloud cover (**m**–**p**, units: %) at 1.5 ℃ (2 ℃; 3 ℃; 4 ℃) GWL under the SSP5-8.5 relative to the recent climate. Dots denote regions where at least 7 out of the 9 models agree in the sign of changes, but only 3 out 5 models in AOD

4.3 The physical processes under the SSP3-7.0

The physical processes for the longwave radiation changes at different GWLs under the SSP3-7.0 are shown in Supplementary Fig. S8. Many characteristics of changes are similar to the processes under the SSP5-8.5 and so are not discussed in detail here. The low-level wind anomalies lead to increased water vapor in the atmosphere over eastern China. The moistening atmosphere is contributing to significant increase of surface clear-sky downward longwave radiation across China.

Considering the role of shortwave radiation under the SSP3-7.0, Fig. 14 shows the future changes of the related variables. There is a distinct difference in the changes of AOD at 550 nm compared with the ones under the SSP5-8.5. The AOD at 550 nm increases significantly over eastern China (Fig. 14a–d), which leads to the reduction of net clear-sky surface shortwave radiation (Fig. 14e–h). Therefore, the net clear-sky surface shortwave radiation plays an opposite role under the SSP3-7.0, which leads to surface cooling. As a result of the decreases in total cloud cover (Fig. 14m–p), the net surface shortwave radiation only increases over the NEC at the 1.5 ℃ and 2 ℃ GWLs (Fig. 14i, j) and the changes of the net surface shortwave radiation over eastern China at the 3 ℃ and 4 ℃ GWLs (Fig. 14k, l) are much weaker and therefore they play a weaker role for surface warming than the

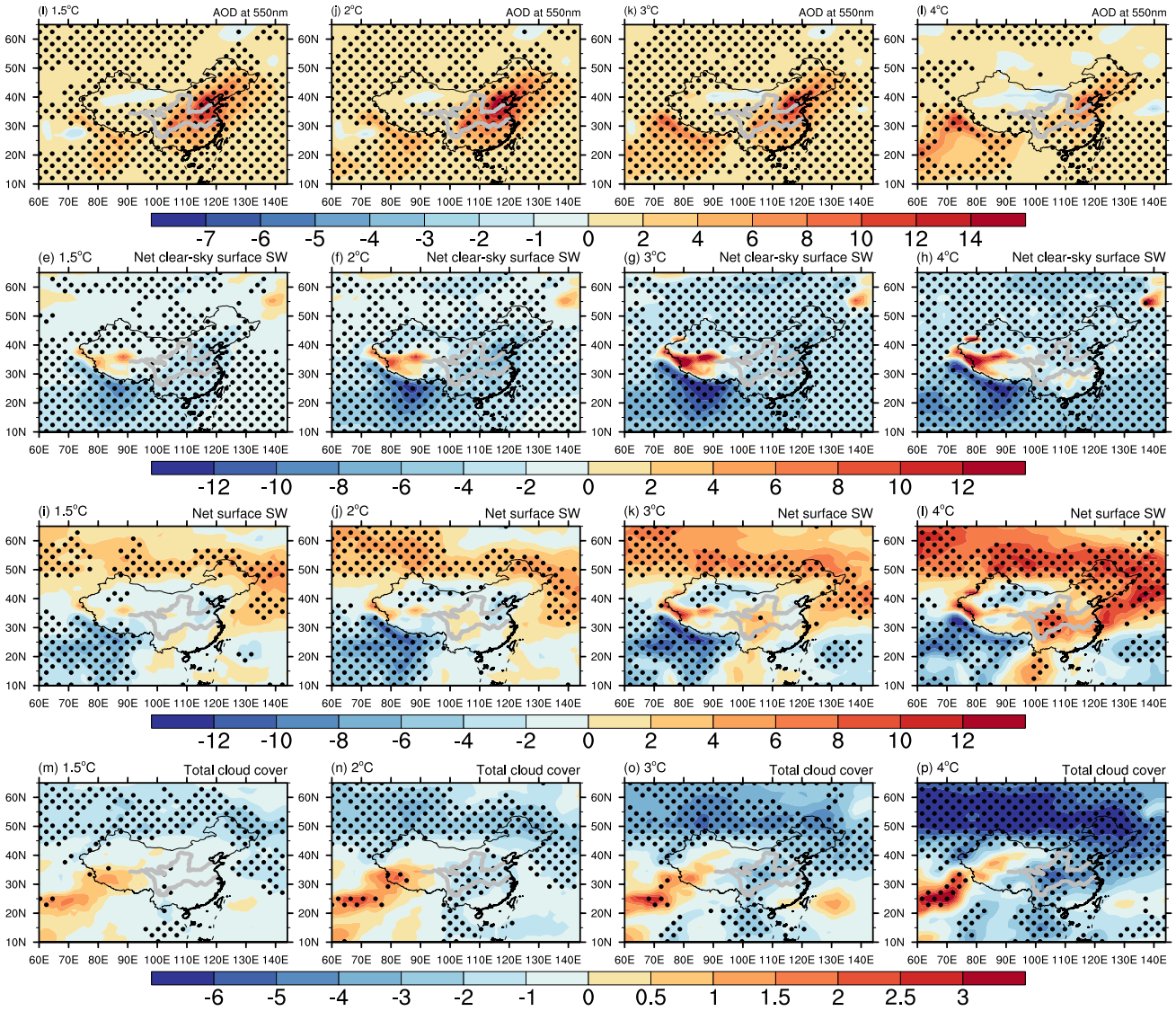

Fig. 14 Spatial distributions of the changes in AOD at 550 nm (**a**–**d**, units: 10^{-3}, results are based on 5 models in which AOD is available), net clear-sky surface shortwave radiation (**e**–**h**, units: W m^{-2}), net surface shortwave radiation (**i**–**l**, units: W m^{-2}), and total cloud cover (**m**–**p**, units: %) at 1.5 ℃ (2 ℃; 3 ℃; 4 ℃) GWL under the SSP3-7.0 relative to the recent climate. Dots denote regions where at least 7 out of the 9 models agree in the sign of changes, but only 3 out 5 models in AOD

ones under the SSP5-8.5. The increased shortwave and longwave radiation over eastern China contribute to increases in both Tmax and Tmin and are responsible for large increases in HW frequency and intensity.

To sum up, the surface warming in summer over China under the SSP3-7.0 is mainly contributed by the increased longwave radiation with weak contribution from changes in net surface shortwave radiation. The seasonal mean surface warming results in enhanced upward sensible and latent heat fluxes, leading to increases in Tmax and Tmin and resulting in the increase of Compound HWs across China.

5 Conclusions

Under the influence of global warming, there will be an increase of warm extremes over China. This study quantified the expected changes in the frequency, intensity, and duration of summer Compound Heat Waves (HWs) over China using CMIP6 simulations and explored the associated physical processes. In particular, the future changes of summer Compound HWs over China is explored at global warming levels (GWLs) representative of changes in global mean surface temperature at the 1.5 ℃, 2 ℃, 3 ℃ and 4 ℃ based on the multi-model ensembles of CMIP6 under the

SSP3-7.0 and SSP5-8.5. The main conclusions can be summarized as follows.

The spatial climatological distributions of the properties of Compound HWs have similar patterns in the recent climate and in the future four GWLs under two scenarios. Therefore, one important conclusion is that the magnitudes and spatial distributions of future changes of Compound HWs are primarily dependent on GWLs and they are not very sensitive to scenarios. The heatwave events over China become more frequent, event temperature becomes hotter, and event duration becomes longer at different GWLs than those in the recent climate. However, the magnitudes of changes increase with increasing GWL. For example, at a 4 ℃ GWL, the frequency of HWs increases by more than fivefold under both scenarios, and the intensity (duration) of HWs averaged under the two scenarios is 2.28 ℃ hotter (3.59 days longer) than those in the recent climate over the entire China. Furthermore, the maximum duration of HW events can reach more than 25 days in summer at 4 ℃ GWL in comparison with 8 days in the recent climate.

Although the changes in frequency, intensity and duration of Compound HW scale broadly across China with GWL, these properties show some regional differences. For example, the increases of the occurrence of Compound HWs over NWC are the largest among the subregions. Furthermore, NEC and NWC show the greatest intensification in intensity and the increases in duration over SWC are much longer than the other regions.

The probability ratios (PRs) of the extreme rare Compound HWs over China increase with increasing GWLs. The 50-year and 100-year rare events are projected to become 1-year event at the 4 ℃ GWL across China. NWC shows the largest PRs of intensity at the 3 ℃ and 4 ℃ GWLs, so that the 50-year (100-year) high-intensity event is projected to become a 1.7-year and 1.1-year (2.7-year and 1.2-year) event in the future. The PRs of duration over SWC are the largest among the subregions and the 50-year and 100-year long-duration events over SWC are projected to become 1-year and 1.2-year events, respectively.

The summer seasonal mean changes in Tmax and Tmin dominates the changes in Compound HW properties over China at the different GWLs. However, the processes leading to the changes in Tmax and Tmin are scenario dependent. Under the SSP5-8.5, the surface warming across China is related to the increases of longwave radiation, partly resulted from increase in greenhouse gas forcing and partly resulted from increased water vapor and the increases of shortwave radiation over eastern China related to decreases in aerosols. The regional variations in the water vapor over China are consistent with atmospheric circulation changes. This seasonal mean surface warming results in enhanced upward sensible and latent heat fluxes, leading to increased summer mean daily maximum and minimum of near-surface air temperature (Tmax and Tmin) and the enhancement of Compound HWs properties over the entire China. Under the SSP3-7.0, the surface warming in summer over China is mainly contributed by the increased longwave radiation with weak contribution from changes in net surface shortwave radiation related to increased aerosol changes under this scenario. The seasonal mean surface warming results in enhanced upward sensible and latent heat fluxes, leading to increases in Tmax and Tmin and resulting in the increase of Compound HWs across China. In terms of the regional differences of changes in HWs properties, the large increases in frequency and intensity are mainly contributed by the longwave and shortwave radiation.

Our results suggest that China would face a future with projected frequency increase, intensity enhancement and duration extension of HWs. Considering the severe impacts of HWs on human well-being and ecosystem (Yin et al. 2023), our results provide important context for the development of mitigation and adaption decisions to reduce the adverse impacts of HWs on society.

This study provides a view on the future changes of summer Compound HWs and the related physical processes at different GWLs. The results are based on multi-model ensembles of CMIP6 and, thus, more robust than results from a single model. Nevertheless, as demonstrated in Fig. 5, there is a large spread of future projections in Compound HWs properties among the models. Unfortunately, the reasons for this model uncertainty are still unclear. Understanding this spread is an important question and needs further study in order to improve predictions of future changes in HWs over China.

Supplementary Information The online version contains supplementary material available at https://doi.org/10.1007/s00382-023-07001-4.

Acknowledgements We acknowledge the international modeling groups for providing their data for analysis, the Program for Climate Model Diagnosis and Inter-comparison (PCMDI) for collecting and achieving the model data, the World Climate Research Programme's (WCRP's) Coupled Model Inter-comparison Project (CMIP) for organizing the model data analysis activity. We would like to thank Prof. Andrew Turner and Dr. Laura Wilcox for providing suggestions which help to improve this paper. The authors greatly appreciate two anonymous reviewers for their constructive comments and suggestions on the early version of this paper.

Author contributions Data collection and analysis were mainly performed by MZ. The first draft of this paper was written by MZ. BD, RS and JR helped to revise the manuscript. All authors read and approved the final manuscript.

Funding BD, RS, and JR are supported by the UK National Center for Atmospheric Science, funded by the Natural Environment Research Council.

Data availability The CMIP6 datasets were obtained from CEDA (https://data.ceda.ac.uk/badc/cmip6/data/CMIP6). The observation data CN05 used in Supplementary file was download from CMA (http://www.nmic.cn).

Declarations

Conflict of interest The authors declared that they have no relevant financial or non-financial interests to disclose.

References

Alizadeh MR, Abatzoglou JT, Adamowski JF et al (2022) Increasing heat-stress inequality in a warming climate. Earth's Futur 10:1–11. https://doi.org/10.1029/2021EF002488

An N, Zuo Z (2021) Changing structures of summertime heatwaves over China during 19 61–2017. Sci China Earth Sci 64:1242–1253. https://doi.org/10.1007/s11430-020-9776-3

Argüeso D, Di Luca A, Perkins-Kirkpatrick SE, Evans JP (2016) Seasonal mean temperature changes control future heat waves. Geophys Res Lett 43:7653–7660. https://doi.org/10.1002/2016GL069408

Boucher O, Randall D, Artaxo P, et al (2013) Clouds and aerosols. In: Climate change 2013: the physical science basis. contribution of working group I to the fifth assessment report of the intergovernmental panel on climate change. 9781107057999:571–658. https://doi.org/10.1017/CBO9781107415324.016

Brás TA, Seixas J, Carvalhais N, Jagermeyr J (2021) Severity of drought and heatwave crop losses tripled over the last five decades in Europe. Environ Res Lett. https://doi.org/10.1088/1748-9326/abf004

Chen W, Dong B (2021) Projected near-term changes in temperature extremes over China in the mid-twenty-first century and underlying physical processes. Clim Dyn 56:1879–1894. https://doi.org/10.1007/s00382-020-05566-y

Chen Y, Li Y (2017) An inter-comparison of three heat wave types in China during 1961–2010: observed basic features and linear trends. Sci Rep 7:2–11. https://doi.org/10.1038/srep45619

Chen Y, Zhai P (2017) Revisiting summertime hot extremes in China during 1961–2015: Overlooked compound extremes and significant changes. Geophys Res Lett 44:5096–5103. https://doi.org/10.1002/2016GL072281

Chen W, Dong B, Wilcox L et al (2019) Attribution of recent trends in temperature extremes over China: Role of changes in anthropogenic aerosol emissions over Asia. J Clim 32:7539–7560. https://doi.org/10.1175/JCLI-D-18-0777.1

Chen H, Sun J, Lin W, Xu H (2020) Comparison of CMIP6 and CMIP5 models in simulating climate extremes. Sci Bull 65:1415–1418. https://doi.org/10.1016/j.scib.2020.05.015

Coumou D, Rahmstorf S (2012) A decade of weather extremes. Nat Clim Chang 2:491–496. https://doi.org/10.1038/nclimate1452

De Bono A, Giuliani G, Kluster S, Peduzzi P (2004) Impacts of summer 2003 heat wave in Europe. Environ Alert Bull UNEP 4

Della-Marta PM, Luterbacher J, von Weissenfluh H et al (2007) Summer heat waves over western Europe 1880–2003, their relationship to large-scale forcings and predictability. Clim Dyn 29:251–275. https://doi.org/10.1007/s00382-007-0233-1

Domeisen DIV, Eltahir EAB, Fischer EM et al (2023) Prediction and projection of heatwaves. Nat Rev Earth Environ 4:36–50. https://doi.org/10.1038/s43017-022-00371-z

Donat MG, Alexander LV, Yang H et al (2013) Updated analyses of temperature and precipitation extreme indices since the beginning of the twentieth century: the HadEX2 dataset. J Geophys Res Atmos 118:2098–2118. https://doi.org/10.1002/jgrd.50150

Douville H, Chauvin F, Broqua H (2001) Influence of soil moisture on the Asian and African monsoons. Part I: mean monsoon and daily precipitation. J Clim 14:2381–2403. https://doi.org/10.1175/1520-0442(2001)014%3c2381:IOSMOT%3e2.0.CO;2

Eyring V, Bony S, Meehl GA et al (2016) Overview of the Coupled Model Intercomparison Project Phase 6 (CMIP6) experimental design and organization. Geosci Model Dev 9:1937–1958. https://doi.org/10.5194/gmd-9-1937-2016

Freychet N, Sparrow S, Tett SFB et al (2018) Impacts of anthropogenic Forcings and El Niño on Chinese extreme temperatures. Adv Atmos Sci 35:994–1002. https://doi.org/10.1007/s00376-018-7258-8

Gershunov A, Cayan DR, Iacobellis SF (2009) The great 2006 heat wave over California and Nevada: Signal of an increasing trend. J Clim 22:6181–6203. https://doi.org/10.1175/2009JCLI2465.1

Gumbel EJ (1942) On the frequency distribution of extreme values in meteorological data. Bull Am Meteorol Soc 23:95–105

Guo X, Huang J, Luo Y et al (2017) Projection of heat waves over China for eight different global warming targets using 12 CMIP5 models. Theor Appl Climatol 128:507–522. https://doi.org/10.1007/s00704-015-1718-1

Hatfield JL, Prueger JH (2015) Temperature extremes: effect on plant growth and development. Weather Clim Extrem 10:4–10. https://doi.org/10.1016/j.wace.2015.08.001

Hatzianastassiou N, Matsoukas C, Drakakis E et al (2007) The direct effect of aerosols on solar radiation based on satellite observations, reanalysis datasets, and spectral aerosol optical properties from Global Aerosol Data Set (GADS). Atmos Chem Phys 7:2585–2599. https://doi.org/10.5194/acp-7-2585-2007

Hu T, Sun Y (2020) Projected changes in extreme warm and cold temperatures in China from 1.5 to 5 °C global warming. Int J Climatol 40:3942–3953. https://doi.org/10.1002/joc.6436

Intergovernmental Panel on Climate Change (IPCC) (2022) The ocean and cryosphere in a changing climate. Ocean Cryosph a Chang Clim. https://doi.org/10.1017/9781009157964

Jehn FU, Schneider M, Wang JR et al (2021) Betting on the best case: Higher end warming is underrepresented in research. Environ Res Lett. https://doi.org/10.1088/1748-9326/ac13ef

Jehn FU, Kemp L, Ilin E et al (2022) Focus of the IPCC assessment reports has shifted to lower temperatures. Earth's Futur 10:1–4. https://doi.org/10.1029/2022EF002876

Kong D, Gu X, Li J et al (2020) Contributions of global warming and urbanization to the intensification of human-perceived heatwaves over China. J Geophys Res Atmos 125:1–16. https://doi.org/10.1029/2019JD032175

Kornhuber K, Coumou D, Vogel E et al (2020) Amplified Rossby waves enhance risk of concurrent heatwaves in major breadbasket regions. Nat Clim Chang 10:48–53. https://doi.org/10.1038/s41558-019-0637-z

Lee JY, Marotzke J, Bala G et al (2021) Future global climate: scenario-based projections and near-term information. IPCC

Lesk C, Rowhani P, Ramankutty N (2016) Influence of extreme weather disasters on Global Crop Production. Nature 529:84–87. https://doi.org/10.1038/nature16467

Li X, Ren G, Wang S et al (2021) Change in the heatwave statistical characteristics over China during the climate warming slowdown. Atmos Res 247:105152. https://doi.org/10.1016/j.atmosres.2020.105152

Liao W, Li D, Malyshev S et al (2021) Amplified increases of compound hot extremes over urban land in China. Geophys Res Lett 48:1–12. https://doi.org/10.1029/2020GL091252

Liu Y, Geng X, Hao Z, Zheng J (2020) Changes in climate extremes in central asia under 1.5 and 2 °c global warming and their impacts on agricultural productions. Atmosphere (basel) 11:1–19. https://doi.org/10.3390/atmos11101076

Luo M, Lau NC, Liu Z (2022) Different mechanisms for daytime, nighttime, and compound heatwaves in southern China. Weather Clim Extrem 36:100449. https://doi.org/10.1016/j.wace.2022.100449

O'Neill BC, Tebaldi C, Van Vuuren DP et al (2016) The Scenario Model Intercomparison Project (ScenarioMIP) for CMIP6. Geosci Model Dev 9:3461–3482. https://doi.org/10.5194/gmd-9-3461-2016

Perkins SE (2015) A review on the scientific understanding of heatwaves-their measurement, driving mechanisms, and changes at the global scale. Atmos Res 164–165:242–267. https://doi.org/10.1016/j.atmosres.2015.05.014

Perkins-Kirkpatrick SE, Lewis SC (2020) Increasing trends in regional heatwaves. Nat Commun 11:1–8. https://doi.org/10.1038/s41467-020-16970-7

Piao S, Ciais P, Huang Y et al (2010) The impacts of climate change on water resources and agriculture in China. Nature 467:43–51. https://doi.org/10.1038/nature09364

Raftery AE, Zimmer A, Frierson DM et al (2017) Less than 2 °C warming by 2100 unlikely. Nat Clim Chang 7:637–641. https://doi.org/10.1038/nclimate3352

Robine JM, Cheung SLK, Le Roy S et al (2008) Death toll exceeded 70,000 in Europe during the summer of 2003. Comptes Rendus - Biol 331:171–178. https://doi.org/10.1016/j.crvi.2007.12.001

Sehler R, Li J, Reager J, Ye H (2019) Investigating relationship between soil moisture and precipitation globally using remote sensing observations. J Contemp Water Res Educ 168:106–118. https://doi.org/10.1111/j.1936-704x.2019.03324.x

Seneviratne SI, Donat MG, Mueller B, Alexander LV (2014) No pause in the increase of hot temperature extremes. Nat Clim Chang 4:161–163. https://doi.org/10.1038/nclimate2145

Singh S, Mall RK, Singh N (2021) Changing spatio-temporal trends of heat wave and severe heat wave events over India: An emerging health hazard. Int J Climatol 41:E1831–E1845. https://doi.org/10.1002/joc.6814

Song Y, Achberger C, Linderholm HW (2011) Rain-season trends in precipitation and their effect in different climate regions of China during 1961–2008. Environ Res Lett. https://doi.org/10.1088/1748-9326/6/3/034025

Song F, Zhang GJ, Ramanathan V, Leung LR (2022) Trends in surface equivalent potential temperature: a more comprehensive metric for global warming and weather extremes. Proc Natl Acad Sci U S A 119:1–7. https://doi.org/10.1073/pnas.2117832119

Su Q, Dong B (2019a) Recent decadal changes in heat waves over China: drivers and mechanisms. J Clim 32:4215–4234. https://doi.org/10.1175/JCLI-D-18-0479.1

Su Q, Dong B (2019b) Projected near-term changes in three types of heat waves over China under RCP4.5. Clim Dyn 53:3751–3769. https://doi.org/10.1007/s00382-019-04743-y

Sun Y, Zhang X, Zwiers FW et al (2014) Rapid increase in the risk of extreme summer heat in Eastern China. Nat Clim Chang 4:1082–1085. https://doi.org/10.1038/nclimate2410

Sun Y, Hu T, Zhang X (2018) Substantial increase in heat wave risks in China in a future warmer world. Earth's Futur 6:1528–1538. https://doi.org/10.1029/2018EF000963

UNFCCC (United Nations Framework Convention on Climate Change). 2015. "Adoption of the Paris Agreement." Conference of the Parties, Paris, France, November 30–December 11

Wang J, Yan Z (2021) Rapid rises in the magnitude and risk of extreme regional heat wave events in China. Weather Clim Extrem 34:100379. https://doi.org/10.1016/j.wace.2021.100379

Wang P, Tang J, Sun X et al (2017) Heat waves in China: definitions, leading patterns, and connections to large-scale atmospheric circulation and SSTs. J Geophys Res Atmos 122:10679–10699. https://doi.org/10.1002/2017JD027180

Wang P, Hui P, Xue D, Tang J (2019) Future projection of heat waves over China under global warming within the CORDEX-EA-II project. Clim Dyn 53:957–973. https://doi.org/10.1007/s00382-019-04621-7

Wang J, Chen Y, Tett SFB et al (2020) Anthropogenically-driven increases in the risks of summertime compound hot extremes. Nat Commun. https://doi.org/10.1038/s41467-019-14233-8

WMO (2013) The global climate 2001–2010: a decade of climate extremes. WMO-No. 1103. World Meteorological Organization, p 119

Xie W, Zhou B, You Q et al (2020) Observed changes in heat waves with different severities in China during 1961–2015. Theor Appl Climatol 141:1529–1540. https://doi.org/10.1007/s00704-020-03285-2

Xie W, Zhou B, Han Z, Xu Y (2021) Projected changes in heat waves over China: ensemble result from RegCM4 downscaling simulations. Int J Climatol 41:3865–3880. https://doi.org/10.1002/joc.7047

Xie W, Zhou B, Han Z, Xu Y (2022) Substantial increase in daytime-nighttime compound heat waves and associated population exposure in China projected by the CMIP6 multimodel ensemble. Environ Res Lett. https://doi.org/10.1088/1748-9326/ac592d

Xu B, Chen H, Gao C et al (2019) Decadal intensification of local thermal feedback of summer soil moisture over North China. Theor Appl Climatol 138:1563–1571. https://doi.org/10.1007/s00704-019-02918-5

Yang X, Zhou B, Xu Y, Han Z (2021) CMIP6 evaluation and projection of temperature and precipitation over China. Adv Atmos Sci 38:817–830. https://doi.org/10.1007/s00376-021-0351-4

Yao Z, Li X, Xiao J (2018) Characteristics of daily extreme wind gusts on the Qinghai-Tibet Plateau, China. J Arid Land 10:673–685. https://doi.org/10.1007/s40333-018-0094-y

Ye DX, Yin JF, Chen ZH et al (2014) Spatial and temporal variations of heat waves in China from 1961 to 2010. Adv Clim Chang Res 5:66–73. https://doi.org/10.3724/SP.J.1248.2014.066

Yin J, Gentine P, Slater L et al (2023) Future socio-ecosystem productivity threatened by compound drought–heatwave events. Springer US

You Q, Cai Z, Wu F et al (2021) Temperature dataset of CMIP6 models over China: evaluation, trend and uncertainty. Clim Dyn 57:17–35. https://doi.org/10.1007/s00382-021-05691-2

Zhang GW, Zeng G, Iyakaremye V, You QL (2020) Regional changes in extreme heat events in China under stabilized 1.5 °C and 2.0 °C

global warming. Adv Clim Chang Res 11:198–209. https://doi.org/10.1016/j.accre.2020.08.003

Zhao W (2020) Extreme weather and climate events in China under changing climate. Natl Sci Rev 7:938–943. https://doi.org/10.1093/nsr/nwaa069

Zhao A, Bollasina MA, Stevenson DS (2019) Strong influence of aerosol reductions on future heatwaves. Geophys Res Lett 46:4913–4923. https://doi.org/10.1029/2019GL082269

Zhou W, Chan JCL, Chen W et al (2009) Synoptic-scale controls of persistent low temperature and icy weather over Southern China in January 2008. Mon Weather Rev 137:3978–3991. https://doi.org/10.1175/2009MWR2952.1

Zhou B, Wen QH, Xu Y et al (2014) Projected changes in temperature and precipitation extremes in China by the CMIP5 multimodel ensembles. J Clim 27:6591–6611. https://doi.org/10.1175/JCLI-D-13-00761.1